

## Measuring White Dwarf Variability from Sparsely Sampled Gaia DR3 Multi-Epoch Photometry

MAYA STEEN,<sup>1,2</sup> J. J. HERMES,<sup>1</sup> JOSEPH A. GUIDRY,<sup>1,\*</sup> ANNABELLE PAIVA,<sup>1</sup> JAY FARIHI,<sup>3</sup> TYLER M. HEINTZ,<sup>1</sup> BRISON B. EWING,<sup>1</sup> AND NATHANIEL BERRY<sup>4</sup>

<sup>1</sup>Department of Astronomy, Boston University, 725 Commonwealth Ave., Boston, MA 02215, USA

<sup>2</sup>Department of Astronomy, New Mexico State University, Las Cruces, NM 88003, USA

<sup>3</sup>Department of Physics & Astronomy, University College London, Gower Street, London WC1E 6BT, UK

<sup>4</sup>Department of Physics and Astronomy, University of North Carolina, Chapel Hill, NC 27599, USA

### ABSTRACT

White dwarf stars are ubiquitous in the Galaxy, and are essential to understanding stellar evolution. While most white dwarfs are photometrically stable and reliable flux standards, some can be highly variable, which can reveal unique details about the endpoints of low-mass stellar evolution. In this study we characterize a sample of high-confidence white dwarfs with multi-epoch photometry from Gaia Data Release 3. We compare these Gaia light curves with light curves from the Zwicky Transiting Facility and the Transiting Exoplanet Survey Satellite to see when Gaia data independently can accurately measure periods of variability. From this sample, 105 objects have variability periods measured from the Gaia light curves independently, with periods as long as roughly 9.5 d and as short as 256.2 s (roughly 4 min), including seven systems with periods shorter than 1000 s. We discover 86 new objects from the 105 target sample, including pulsating, spotted, and binary white dwarfs, and even a new 68.4 min eclipsing cataclysmic variable. The median amplitude of the absolute photometric variability we confirm from Gaia independently is 1.4%, demonstrating that Gaia epoch photometry is capable of measuring short-term periods even when observations are sparse.

### 1. INTRODUCTION

As the endpoints of all stars below roughly  $8 M_{\odot}$ , white dwarfs are extremely common. Their ubiquity and relative simplicity mean that white dwarf stars play an important role as flux standards, which are needed for precise absolute photometry and spectroscopy (e.g., Calamida et al. 2022).

Roughly 97% of all apparently isolated white dwarfs are empirically stable to less than 1% variability on weeks-long timescales (Hermes et al. 2017a). When white dwarfs are photometrically variable they can reveal unique physical properties such as the presence of magnetism or surface rotation periods (e.g., Maoz et al. 2015), binary properties (e.g., Holberg & Howell 2011), remnant planetary systems (e.g., Hallakoun et al. 2018; Guidry et al. 2021), or even their interiors through asteroseismology (e.g., Romero et al. 2012).

Binary systems with at least one white dwarf star can tell us about stellar ages and close binary evolution (e.g., Rebassa-Mansergas et al. 2007; Heintz et al. 2022). These objects can also be progenitors of Type Ia supernovae, which are important distance indicators (Maoz et al. 2015). Binaries with short periods (less than roughly 1 hour) are also potential

candidates for gravitational waves detectable with the Laser Interferometer Space Antenna (LISA, Burdge et al. 2020).

There are a number of ways binaries with a white dwarf can be photometrically variable. Eclipsing systems are the most dramatic, where one star passes in front of the other (e.g., Hallakoun et al. 2016). Eclipsing white dwarfs, which can be used to measure the masses and radii of the system components (Parsons et al. 2017, 2018), are still relatively rare so any increase in the sample is valuable. Eclipses are not necessary to detect close binaries, as hot stars in the system can create a reflection effect from reprocessed heating off a cool companion (e.g., Schaffenroth et al. 2022). In addition, cataclysmic variables (CVs) are highly variable white dwarfs with stochastic mass-transfer from a Roche-lobe-filling main-sequence companion (Warner 1995).

Magnetic white dwarfs can also exhibit strong photometric changes, such as cold (e.g., Brinkworth et al. 2013; Kilic et al. 2015) or hot (e.g., Hoard et al. 2018) spots corresponding to the surface rotation period. Measuring these rotation periods can help to investigate the angular momentum loss during white dwarf formation (Fuller et al. 2019).

Pulsating white dwarfs are variable due to non-radial pulsations as they cool through different instability strips that depend on their surface composition (Winget & Kepler 2008a; Fontaine & Brassard 2008; Hermes et al. 2017c). With enough identified pulsation modes, asteroseismology affords

\* NSF Graduate Research Fellow

**Table 1.** Summary table of the full sample and a subset of Gaia-detected variable candidate white dwarfs.

	Full Sample	Gaia Period Match
Variable objects near white dwarfs in CMD ("Variable candWDs")	1333	105
Candidate WDs with $P_{WD} > 0.75$	1217	104
Variable candWDs with spectroscopic confirmation	568	36
Variable candWDs that are known binaries	91	8
Variable candWDs that are known pulsating WDs	49	2
Variable candWDs known to have magnetic spots	12	8
Variable candWDs with TESS data	698	65
Variable candWDs with ZTF data	992	72

the opportunity to significantly constrain the interiors of white dwarfs, including global rotation rates (e.g., [Hermes et al. 2015, 2017b](#)) and core composition (e.g., [Giannicchele et al. 2018; Chidester et al. 2022](#)).

Motivated by the need to find and constrain new variable white dwarfs, we analyze here a new data product from Gaia Data Release 3 (DR3), which features multi-epoch light curves for sources classified as variable via a machine learning algorithm trained on constant objects ([Eyer et al. 2023](#)). This new Gaia DR3 dataset includes photometric time series in the Gaia  $G$ ,  $G_{BP}$ , and  $G_{RP}$  bands. Previous efforts have focused on literature cross-matches of DR3 variables ([Gavras et al. 2023; Rimoldini et al. 2023](#)), as well as specific object types ([Gaia Collaboration et al. 2023a; Marton et al. 2023](#)).

In Section 2 we discuss our target selection for variable white dwarfs in Gaia DR3, and in Section 3 describe our period-finding analysis. In Section 4 we explain our classification of new white dwarf variables, including new (eclipsing) binaries, spotted (magnetic) white dwarfs, and pulsating white dwarfs, all with coherent periodicities detected from Gaia DR3 photometry independently and confirmed in multiple datasets. We discuss the strengths and limitations of Gaia for period analysis in Section 5 and conclude in Section 6.

## 2. TARGET SELECTION AND OBSERVATIONS

We set out to select and analyze all apparently isolated white dwarf stars flagged as photometrically variable in Gaia DR3 ([Gaia Collaboration et al. 2023b](#)). A new, expanded data product in DR3 is the release of multi-epoch, multi-color ( $G$ ,  $G_{BP}$ ,  $G_{RP}$ ) light curves for roughly 10.5 million objects with anomalously large scatter in their many Gaia visits (a.k.a. transits) that make them high-probability candidate variables ([Eyer et al. 2023](#)). These objects are cataloged in Gaia DR3 with the entry `phot_variable_flag` set to `VARIABLE`; full light curves are available through the Gaia Datalink Service ([Cánovas & de Bruijne 2022](#)), which we accessed using `astroquery.gaia` ([Ginsburg et al. 2019](#)).

In order to focus on isolated white dwarfs, we first restrict the 10.5 million variables in DR3 to be near the white dwarf region of the Gaia color-magnitude diagram by requiring  $M_G > (4.5 \times G_{BP} - G_{RP}) + 9.0$ , similar to the absolute magnitude selection of [Hollands et al. \(2018\)](#). This excludes many white dwarfs in close binaries, such as CVs ([Pala et al. 2020](#)) and post-common-envelope (WD+dM) binaries.

We then cross-match this down-selected sample with the Gaia DR3 catalog of candidate white dwarfs of [Gentile Fusillo et al. \(2021\)](#). This cross-match results in a final sample of 1333 objects, 1217 of which are high-confidence single white dwarfs (with  $P_{WD} > 0.75$ , see Table 1); only 42 objects have  $P_{WD} < 0.3$ . We expect minor contamination from our color cuts from non-isolated white dwarfs, especially CVs with low-luminosity donors.

We further cross-match this sample with the Montreal White Dwarf Database ([Dufour et al. 2017](#)) and SIMBAD ([Wenger et al. 2000](#)) by matching coordinates for each source (precessing the Gaia DR3 epoch to J2000). This cross-match was done in order to collect as much supporting information as possible including literature references and spectroscopic classifications. Relevant information found in this cross match is listed in Table 2.

We compare the Gaia multi-color light curves of our 1333 objects with two other long-baseline photometric surveys. First, we use the Python package `Lightkurve` ([Lightkurve Collaboration et al. 2018; Saunders 2020](#)) to download any 20-second- and 2-min-cadence PDCSAP light curves of our objects as seen by the Transiting Exoplanet Survey Satellite (TESS, [Ricker et al. 2015](#)). This provides at least one month of nearly continuous TESS data for 698 objects in our sample, most brighter than roughly  $G = 17.0$  mag.

Where available, we also download light curves within a 1.4-arcsecond search radius of our targets from Data Release 12 of the Zwicky Transient Facility (ZTF, [Bellm et al. 2019](#)). This provides long-baseline ZTF observations for 992 objects across all magnitudes in our sample, all with declinations north of  $-20$  degrees. We also search for light curves

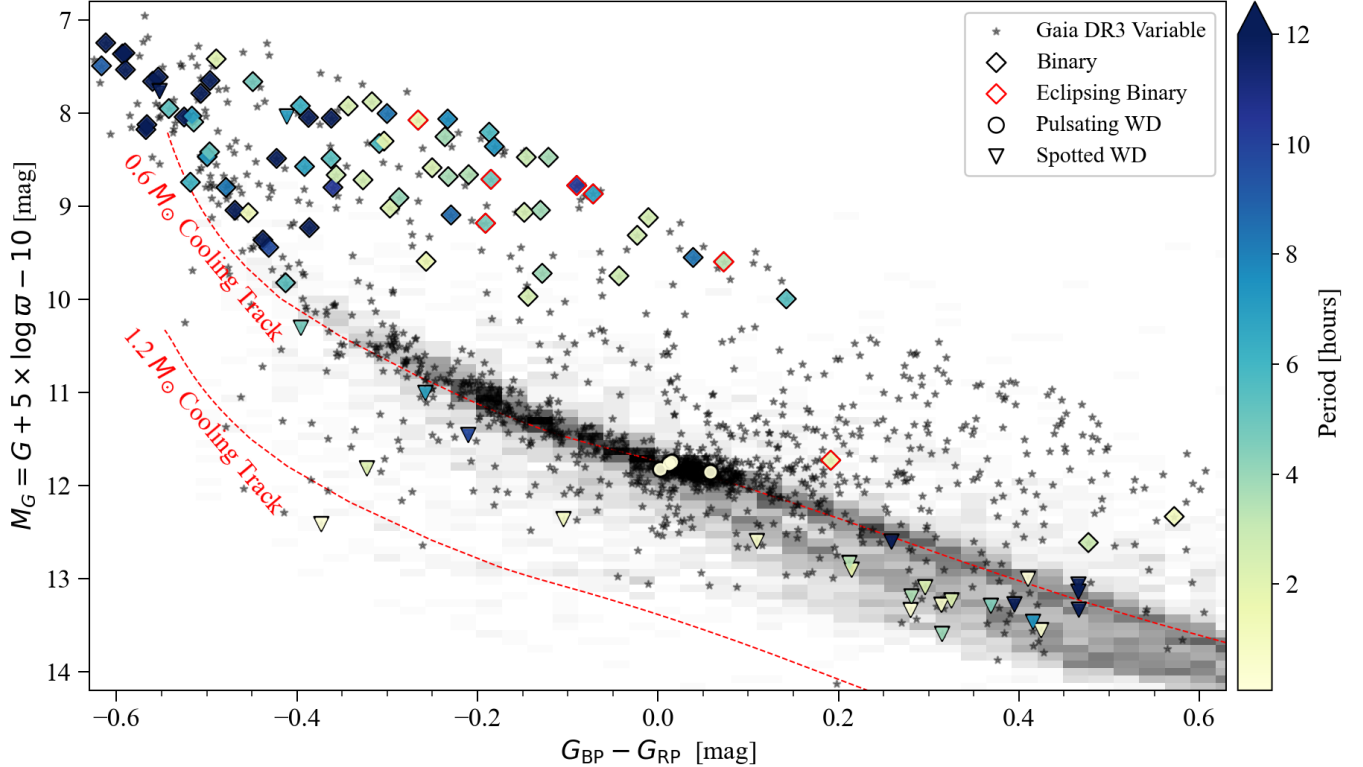


**Figure 1.** Color-magnitude diagram showing our sample of 1333 high-confidence white dwarf candidates flagged as photometrically variable in Gaia DR3 as black stars. The larger colored symbols show the 105 objects discussed in this manuscript which have variability periods measured from their Gaia light curves independently; the color for each point corresponds to the corresponding variability period. The background of this plot is a two-dimensional histogram of white dwarfs within 200 pc matching the magnitude distribution of the 1333 photometrically variable white dwarfs. Dashed red lines show the expected cooling tracks of a  $0.6 M_{\odot}$  white dwarf at top and  $1.2 M_{\odot}$  white dwarf at bottom; white dwarfs cool from the upper left to the lower right in this diagram.

in the south from the All-Sky Automated Survey for SuperNovae (ASAS-SN, Shappee et al. 2014; Kochanek et al. 2017) and the Asteroid Terrestrial-impact Last Alert System (ATLAS, Tonry et al. 2018) projects. However, any objects without TESS photometry in the south mostly had upper limits on photometry due to their faintness, so we did not use their light curves in our analysis here.

### 3. PERIOD-FINDING ANALYSIS

We analyze the Gaia light curves and ZTF and TESS light curves, when available, simultaneously. All available light curves are visually inspected for signatures of variability in both the time and frequency domain, informed by the spectroscopic classification of the white dwarf if known.

We analyze every light curve in the frequency domain by computing Lomb-Scargle periodograms (Astropy Collaboration et al. 2013) using astropy (Astropy Collaboration et al. 2013, 2018, 2022). We also separate the light curves by band-pass filters ( $G$ ,  $G_{BP}$ ,  $G_{RP}$ ,  $g$ ,  $r$ ,  $T$  from Gaia, ZTF, and TESS, respectively) to search for color-dependant variability. We initially classify frequencies as significant if their

amplitude exceeds five times the mean amplitude of all frequencies in the periodogram, a relatively conservative limit given prior sporadically sampled datasets (Breger et al. 1993; Guidry et al. 2021). For simplicity, we use a constant frequency step size for Gaia and ZTF data:  $10^{-8}$  Hz, which corresponds to a critical sampling of 1157 days, consistent with the length of the typical Gaia and ZTF datasets. The step size for the TESS periodogram frequencies is set by the inverse of the TESS light curve baseline, oversampled by a factor of 10. All periodograms are computed to the TESS 2-min Nyquist frequency of  $4160 \mu$ Hz.

We use all available survey information in addition to our coherent period analysis to attempt to classify as many variable candidate white dwarfs in our sample as possible (see Figure 1 and top-line summary in Table 1). The amount of information differs significantly from source to source. For example, only 586 of 1333 objects have a spectral type in the literature listed from either MWDD (Dufour et al. 2017) or SIMBAD (Wenger et al. 2000). Therefore, our classification for 86 of 105 objects in Table 2 listed as “likely” is based on the limited information available and requires spectroscopic follow-up to truly confirm the variability classification.

**Table 2.** Literature information for the 105 white dwarfs in this study with significant variability measured from their Gaia DR3 light curve.

Class (This Work)	Gaia Source ID (DR3)	WD J Name <sup>†</sup> (J2016)	RA (J2016)	DEC (J2016)	<i>G</i> [mag]	$P_{\text{WD}}^{\ddagger}$ [K]	$T_{\text{eff}}^{\ddagger}$ [K]	Mass <sup>†</sup> $[M_{\odot}]$	Sp. Type [pe]	Dist. [pc]	Class <sup>‡</sup>	Score <sup>‡</sup>	$N_G^{\ddagger}$ ( <i>G</i> )	$N_g^{**}$ ( <i>G</i> )	Skew <sup>‡</sup>	IQR <sup>‡</sup> [hr]	$N_{G,S}^*$	Abbe*	$P_{G,S}^*$ [hr]	$P_{\text{lit}}$ [hr]	Ref.
Likely Binary	2789903539324180736	WD J003213.13+160434.78	8.054739	16.07395	15.7	0.982	25410.0	0.24	DO	415.3	WD	0.6	50	68.0	0.755	0.036	50.0	0.836	21.780583	1	
Likely Binary	2317319612801000446	WD J003449.86-392552.69	8.707896	-31.497956	16.1	0.882	14770.0	0.2	DA	431.1		39	58	491.0	-0.416	0.133	39.0	0.822	2.316749	2	
Likely Binary	52242316397099048	WD J011053.06+604933.03	17.721109	60.805856	17.0	0.949	50.2			301.7			58	-0.088	0.068	58.0	0.872	8.361964			
Likely Binary	3233424506701648	WD J012838.99+365436.63	22.12078	38.910093	15.9	0.998	38310.0	0.54	DA	236.1	WD	0.651	30	375.0	-0.396	0.025				3	
Likely Binary	2478893842934875126	WD J013148.02+055900.14	22.950116	-5.983399	17.3	0.939	96630.0	0.63		930.9	WD	0.465	44	329.0	-0.49	0.041					
Likely Binary	459237630766766726	WD J022704.24+591502.04	36.768826	59.25064	15.9	0.988	73600.0	0.51	DA	37.7	WD	0.52	48	420.0	0.282	0.029				4	
Likely Binary	4846154678323892348	WD J03205.10-472106.46	50.521313	-47.51787	17.3	0.978				970.5	WD	0.501	48	0.465	0.121						
Likely Binary	1177703481927936	WD J032803.02+265151.65	52.012578	26.861324	18.2	0.98				656.2	WD	1.0	27	426.0	-0.095	0.16					
Likely Binary	2351846482841688	WD J032902.63+590346.87	52.260969	39.061346	18.6	0.973				876.2	WD	0.5	41	251.0	-0.841	0.082	42.0	0.984	4.038734		
Likely Binary	50906058320056251776	WD J03584.52+213813.74	59.360498	-21.637194	17.8	0.938	24810.0	0.24		802.3		76	242.0	-0.302	0.147	77.0	0.924	1.795123			
Likely Binary	4681729610697929360	WD J041033.37-585203.63	62.639044	-58.867634	17.6	0.94	15430.0	0.13		659.0		39	-0.386	0.175	39.0	0.902	2.8736527				
Likely Binary	320435273173751728	WD J041043.75-041702.63	67.17023	-42.84043	17.9	0.854	28220.0	0.24		1021.7		34	68.0	0.302	0.171	34.0	0.911	2.432582			
Likely Binary	323048971974872192	WD J043823.74-03117.01	69.3636517	5.521344	17.5	0.981	94280.0	0.75		635.9	WD	0.437	53	570.0	-0.394	0.037					
Likely Binary	297468050223581712	WD J050433.01-213097.93	76.37575	-21.502202	18.1	0.959				1208.7	WD	0.252	51	171.0	-0.096	0.107	53.0	0.941	15.0267735		
Likely Binary	33411843546079424	WD J053632.07+2328.65	84.133666	12.524682	16.4	0.979	19510.0	0.25		291.4		48	317.0	-0.347	0.141	50.0	0.906	3.8008657	2,2251		
Likely Binary	294180036292110928	WD J06224.26-191111.75	93.142763	-19.18675	18.0	0.984	23960.0	0.33		640.1	WD	0.5	48	188.0	-0.096	0.115					
Likely Binary	5549322119820590208	WD J06181.57-27.512035.52	94.563662	-51.384787	15.9	0.998	30420.0	0.5		194.3	WD	0.639	36	1.031	0.024						
Likely Binary	31258971987565904	WD J063316.01+013012.78	100.816765	0.996	93720.0	0.83	DO			251.9	WD	0.318	24	300.0	0.06	24.0	0.817	6.0384346	6		
Likely Binary	55750116470244992	WD J063753.57-403756.16	101.91372308	40.632249	17.7	0.987				862.7		43	-0.232	0.15	44.0	0.931	7.015154				
Likely Binary	528622722818008576	WD J063753.57-403756.16	102.0090505	-63.774491	17.5	0.917	22690.0	0.23		691.9		45	-0.084	0.136	45.0	0.917	3.7701112				
Likely Binary	10990503208997984	WD J070617.52+613350.31	106.698306	61.563912	13.5	0.984				158.0		64	915.0	-0.414	0.02	64.0	0.837	8.9701518			
Likely Binary	9890598605065320	WD J071214.74-564308.41	110.444764	56.735666	18.8	0.983	13400.0	0.23		651.7		32	41.0	0.164	0.093	32.0	0.947	2.7708059			
Likely Binary	5615892605641647224992	WD J071312.39+595737.01	112.339236	59.960251	16.1	0.988				424.5	WD	0.273	43	550.0	-0.417	0.088	44.0	0.937	5.3139633	7	
Likely Binary	5615892605641647224992	WD J071316.04-224625.86	115.126834	-22.468245	19.0	0.831	38940.0	0.39		1534.0		69	139.0	-0.59	0.196	71.0	0.919	8.289411			
Likely Binary	521692480396132192	WD J091802.27-634629.78	135.669175	-74.391845	17.2	0.881	10270.0	0.15		278.8	WD	0.559	38	-0.111	0.036						
Likely Binary	3842377248804277168	WD J091748.20+001014.72	139.17023	0.178195	17.4	0.998	34570.0	0.56		406.2	WD	0.606	36	237.0	0.155	0.069					
Likely Binary	543778604539569520	WD J09361.12-340059.16	144.046282	-34.016386	17.1	0.929	49990.0	0.41		649.3		96	-0.357	0.042	97.0	0.92	20.8380564				
Likely Binary	38348939825628900	WD J100635.76+03204.48	151.690524	0.534619	16.7	0.98	15890.0	0.21	DA	336.9	CV	0.382	26	238.0	-0.622	0.083					
Likely Binary	54561270520342352	WD J101228.94-295308.20	163.120558	-29.885268	17.3	0.996	92120.0	0.83		510.5		49	-0.548	0.049	49.0	0.923	8.270957				
Likely Binary	539095784073011872	WD J101318.00-401544.50	165.8325071	-40.1544.50	15.1	0.982				310.3		42	-0.099	0.182	42.0	0.932	0.88348				
Likely Binary	538383283018956032	WD J112355.21-40064.63	170.979607	-40.103915	14.9	0.979				319.2		50	-0.584	0.045	50.0	0.847	16.9484344				
Likely Binary	537856283659002624	WD J111382.79-455817.73	174.635655	-43.971582	16.5	0.981				611.8	WD	0.552	61	-0.176	0.076	61.0	0.893	13.268409			
Likely Binary	607620525994381040	WD J121622.61-545907.30	184.094154	-54.98536	18.7	0.956	17070.0	0.24		748.2		66	-0.378	0.046	67.0	0.888	2.5750154				
Likely Binary	172629792493802400	WD J123955.40-834707.51	189.579829	83.785334	19.8	0.708	7020.0	0.27		333.9	CV	0.716	27	32.0	0.544	0.796					
Likely Binary	35094350718635288	WD J125005.11-203632.29	192.521286	-20.60946	17.4	0.992				699.1	WD	0.577	29	222.0	-0.571	0.129					
Likely Binary	3721943204282387456	WD J13552.52-405864.42	197.845966	8.945966	17.5	0.979	26600.0	0.32	DA	594.8		43	-0.420	0.054	42.0	0.905	2.7448209	2,74511			
Likely Binary	1671880139535324208	WD J140330.89-671255.16	210.876313	67.215334	18.7	0.953	16210.0	0.17		1042.8		60.5	-0.334	0.1	43.0	0.906	3.447414				
Likely Binary	1268054276353808	WD J144007.60+31541.02	220.031656	31.903652	17.3	0.992				670.6		96	692.0	-0.477	0.055	97.0	0.978	23.2777485			
Likely Binary	577338381714683776	WD J145623.30-793654.99	224.096814	-79.615325	17.5	0.926				934.8		58	-0.314	0.155	58.0	0.92	4.819797				
Likely Binary	58730133222069984	WD J145817.91-651024.94	224.574476	-65.173657	17.7	0.957	38640.0	0.42		635.7		88	-0.317	0.074	89.0	0.898	3.679142				
Likely Binary	1728880879608190592	WD J15028.82-4874848.48	226.130353	23.505033	29.141305	18.9	0.945	22570.0	0.25	DAH	1132.5		74	446.0	-0.306	0.056					
Likely Binary	17287083853394704	WD J15012.07+29028.96	224.601506	46.95953	17.5	0.937	18100.0	0.18		640.1		640.1	-0.019	0.226	74.0	0.848	3.7342113				
Likely Binary	209549094287808256	WD J182243.45+35451.42	278.181011	35.755123	18.1	0.994	24510.0	0.42		503.6	WD	0.264	45	1602.0	-0.302	0.069					
Likely Binary	214488090240525568	WD J18506.31-50541.25	281.276271	50.903336	17.8	0.911	18230.0	0.16		830.7		45	1033.0	-0.512	0.105	45.0	0.955	5.7331055			
Likely Binary	2126940892444693760	WD J191931.09+443245.88	289.879471	44.54546	16.6	0.926	33990.0	0.3	CV	535.7	WD	0.5	41	956.0	0.19	0.071	41.0	0.794	6.2207431	14	

**Table 2 continued**

## VARIABLE WHITE DWARFS IN GAIA DR3

**Table 2 (continued)**

Class	Gaia Source ID	WD J Name <sup>†</sup>	RA	DEC	<i>G</i>	$P_{\text{WD}}^{\dagger}$	$T_{\text{eff}}^{\dagger}$	Mass <sup>†</sup>	Sp. Type	Dist.	Class <sup>‡</sup>	Score <sup>‡</sup>	$N_G^{\ddagger}$	$N_g^{**}$	Skew <sup>‡</sup>	IQR <sup>‡</sup>	$N_{G,S}^*$	Abe*	$P_{G,S}^*$	$P_{\text{lit}}$	Ref.
(This Work)	(DR3)	(J2016)	(J2016)	[mag]	[K]	[ $M_{\odot}$ ]	[pe]						( $G$ )	( $G$ )					[hr]	[hr]	
Likely Binary	180730914-7099442432	WD J 195952-094-143534.17	299.970566	14.592818	17.5	0.994	13230.0	0.14	643.8	51	329.0	-0.138	0.05	52.0	0.905	7.1919534					
Likely Binary	1809460380271029344	WD J 200937-024-16521912	302.4034376	16.8	0.949	36520.0	0.72	341.6	61	87.0	-0.119	0.166	62.0	0.938					2.49783		
Likely Binary	200141669527851908	WD J 202354.51-493212.12	305.143844	17.4	0.999	36520.0	0.72	326.4	46		-0.63	0.079	47.0	0.886	5.3152144						
Likely Binary	66779158838046833.36	WD J 202354.90-433513.67	305.143844	17.0	0.976	902.0	WD	0.515	49		-0.07	0.107									
Likely Binary	1863757043284-227384	WD J 202841-38-325837.35	307.172333	32.976997	17.5	0.92	758.4		453.0	56		-0.135	0.378	56.0	0.883	19.4392732					
Likely Binary	6910676050839449728	WD J 1201010.17-052751.14	31.5.29212	-5.464319	14.8	0.998	36900.0	0.52	DBA	140.5	WD	0.662	58	58.0	0.868	12.8902533					
Likely Binary	217729739113097792	WD J 1020840.53-554502.63	317.168856	55.750555	18.9	0.939	8530.0	0.52	180.9	53	613.0	-0.135	0.133	53.0	0.873	2.7846556	15				
Likely Binary	18678518694010050960	WD J 211587-38-364255.40	318.989974	18.0	0.978	773.2		60		477.0	-0.114	0.094	61.0	0.889	6.7479039						
Likely Binary	1958573244454106100	WD J 213119(93-4345)46.84	322.833067	34.879639	17.5	0.984	48120.0	0.54	547.8	68	373.0	-0.601	0.073	69.0	0.985	10.5988838					
Likely Binary	26673179173745944	WD J 213988.29-074126.17	324.992963	-7.690733	16.7	0.99	517.2	WD	0.5	224.0	-0.197	0.093							9.91934		
Likely Binary	200078553962275104	WD J 221545.15-503759.46	333.938098	50.6313181	18.1	0.967	847.4		54.0	55.0	0.126	0.129	54.0	0.913	5.4185123						
Likely Binary	28338498020559360	WD J 24559.39-301635.35	341.414024	20.275955	15.7	0.994	14490.0	0.26		157.0	WD	0.296	36	771.0	0.024						
Likely Binary	2606828079159380992	WD J 224653.73-094834.48	341.724022	-9.809701	16.4	0.982	DA		525.7	WD	0.62	23	82.0	-0.134	0.038				17		
Likely Binary	66098807867820512	WD J 212626.39-274012.56	303.026633	16.7	0.993	72550.0	0.65	447.8	32	268.0	-0.316	0.137	32.0	0.835	5.1362607						
Likely Binary	241152965735936900	WD J 230047.06-125054.98	345.196258	-12.848088	16.7	0.995	34300.0	0.51	DB	310.9	WD	0.686	26	244.0	-0.148	0.053			18		
Likely Binary	221018054096762624	WD J 123411.66-363053.05	351.046663	65.514762	16.1	0.932	32760.0	0.27	356.7	WD	1.0	558.0	0.109	0.108	54.0	0.858	7.2978032				
Likely Binary	6523373973310305664	WD J 233923.79-485350.19	354.849218	-48.897269	17.0	0.978	24160.0	0.27	454.1	S	0.157	78	-0.36	0.095	78.0	0.914	2.530295				
Likely Eclipsing Binary	4148134390073-094834.48	WD J 005052.55-503408.46	11.25983	50.568959	17.6	0.955	19200.0	0.23	557.1	53	585.0	0.153	0.098	55.0	0.912	1.8351055					
Likely Eclipsing Binary	688616512688802176	WD J 130905.43-470852.39	197.272675	-47.147918	18.3	0.908	11040.0	0.13	542.4	49		3.648	0.18	50.0	0.817	0.5338734					
Likely Eclipsing Binary	688616512688802164	WD J 154008.28-392917.61	235.034874	-39.488217	17.3	0.973	9590.0	0.41	131.9	CV	0.067	48	4.052	0.095	49.0	0.6007557	3.48				
Likely Eclipsing Binary	205636807603855360	WD J 005032.64-350525.08	307.048487	35.090314	17.9	0.955	20320.0	0.23	670.1	52	610.0	-0.316	0.079	52.0	0.901	10.3938399					
Likely Eclipsing Binary	38056904467742768	WD J 005332.64-385276.78	38.924991	18.3	0.956	20540.0	0.24	841.3	40	828.0	-0.285	0.113	40.0	1.002	4.849611	4.86			20		
Known Eclipsing Binary	5785394139073-094834.48	WD J 008746.18-034255.35	134.442416	37.153899	18.3	0.872	21040.0	0.19	DA	1088.4	72	209.0	1.739	0.235	73.0	0.874	1.56231667	21.22			
Known Eclipsing Binary	1446230735421615872	WD J 132518.18-233808.02	201.235817	23.635475	18.2	0.983	17000.0	0.24	DA+IM	621.7		52	459.0	-0.328	0.077	52.0	0.944	4.67590375	23.24		
Known Binary	111217031099852926	WD J 071709/79-740040.53	109.294866	74.01089	15.0	0.996	14340.0	0.29	DA	101.3	WD	0.469	58.0	-0.331	0.025	58.0	0.796	2.473008	25		
Known Binary	560000875757586928	WD J 095017.97-251124.79	147.574789	-25.190355	15.5	0.888	19340.0	0.16	DA+IM	309.8	WD	1.0	42.0	0.346	0.068	42.0	0.96	7.6478424	7.647696	26.27	
Known Binary	12399857610743648832	WD J 155938.12-272606.84	217.0159	16.6	0.955	24650.0	0.24	DA	447.5	WD	0.5	113	204.0	-0.044	116.0	0.865	5.7252728	5.7252333	28.29		
Likely CV	618386018127234432	WD J 113007.78-234432.33	195.073434	-32.968155	20.3	0.851	DA	590.8	CV	906.0	31		-0.253	0.176					30		
Known CV	589948280590492288	WD J 03141.14-232342.92	48.558844	-22.595499	18.2	0.996	10710.0	0.66	CV	160.4	WD	0.578	31.0	-0.763	0.107	31.0	0.877	1.35	31.32		
Known CV	5645504991845229396	WD J 083843.35-262701.14	129.886058	-28.450262	17.6	0.978	9500.0	0.41	CV	156.6	S	0.6	77	0.232	0.847	77.0	0.513	16.1135388	1.64021667	33.34	
Likely DAV	5709854047291834496	WD J 108292.44-163337.25	127.353247	-16.560327	17.6	0.996	10930.0	0.58	DA	141.4	40	140.0	-0.599	0.069	41.0	0.724	1.0316165	35			
Likely DAV	34597002527986448	WD J 120650-89-360549.23	181.171597	-38.097216	15.7	0.998	9187.0	0.65	DA	47.4	79	393.0	-1.407	0.026	79.0	0.725	0.56698	0.07116667	36.37		
Known DAV	2026655131220381824	WD J 119227.88-381340.59	25.158763	15.1	0.998	1170.0	0.6	DA	61.1	DA	0.761	62	0.409	0.026	62.0	0.88618611	0.08618611	38,39			
Likely Spot	641050192353186928	WD J 211823.88-585353.53	329.590553	15.8	0.998	11640.0	0.61	DA	63.7	WD	0.761	42	219.0	0.293	0.069	42.0	0.897	4.4630736	45		
Likely Spot	313206675129937408	WD J 001157.12+143337.67	17.987841	31.608892	16.9	0.999	18120.0	0.8	DA	125.3	WD	0.355	32	281.0	0.158						
Likely Spot	513988051029408768	WD J 1018292.02-195446.58	24.634396	-19.912219	15.5	0.994	8430.0	0.93	DA	24.4		62	179.0	0.201	0.032	62.0	0.933	3.9428678	40		
Likely Spot	105601048101988992	WD J 020322.94-255855.90	30.945858	25.981003	18.1	0.992	9210.0	0.64	DAH	124.9	WD	0.569	26	69.5	0.129						
Likely Spot	461886023015095408	WD J 020322.94-255855.90	40.651134	-82.110184	16.4	0.995	9450.0	0.79	DA	53.1	WD	0.549	42	0.711	0.035	42.0	0.91	3.3447333	41		
Likely Spot	1875760083144704	WD J 052026.55-381340.59	15.4	1.0	19830.0	0.993	8770.0	0.83	DA	74.6	WD	0.562	28	407.0	-0.391	0.017			42		
Likely Spot	29513807999136192	WD J 01062555.04-141442.31	96.479499	-14.245324	16.5	0.994	8020.0	0.74	DAH	43.9	WD	0.509	42	219.0	0.242	0.069					
Likely Spot	3161684705268192	WD J 072758.87+01.15.08	10.198911	17.4	0.995	7600.0	0.77	DAH	58.8	WD	0.331	24	286.0	0.242	0.027						
Likely Spot	10302897128189296	WD J 083531.17-533324.91	128.879468	53.541364	18.2	0.992	8490.0	0.8	DAH	96.7	WD	0.536	35	75.0	-0.382	0.065					
Likely Spot	562076437599189376	WD J 090212.89-394553.32	135.554166	-39.764881	16.0	0.993	8770.0	0.83	DAH	36.4	WD	0.586	57		-0.027	0.024					
Likely Spot	359848249175393888	WD J 1115033.33-303618.81	177.653767	-6.603565	16.4	0.993	8770.0	0.89	DA	41.5	WD	0.509	48	130.0	0.259	0.026			44		
Likely Spot	14652141733690376	WD J 124740.10-303007.41	191.91707	30.501779	17.9	0.992	7460.0	0.65	DA	82.3	WD	0.632	41	548.0	-0.381	0.042			45		
Likely Spot	627901447402485632	WD J 144410.08-214338.33	221.041685	-21.72792	16.9	0.999	25120.0	1.12		106.0	WD	0.777	22	102.0	0.454	0.045					
Likely Spot	163900764701426176	WD J 154801.37-62361.57	237.005479	18.6	0.999	30150.0	0.75	449.5	ECL	0.005	57	984.0	0.369	1.055			9.474283333	46			
Likely Spot	43346156247723712	WD J 163335.21-1001.16.33	253																		

**Table 2 (continued)**

Class	Gaia Source ID	WD J Name <sup>†</sup>	RA	DEC	<i>G</i>	$P_{\text{WD}}^{\dagger}$	$T_{\text{eff}}^{\dagger}$	Mass <sup>†</sup>	Sp. Type	Dist.	Class <sup>‡</sup>	Score <sup>‡</sup>	$N_G^{\ddagger}$	$N_g^{**}$	Skew <sup>‡</sup>	$IQR^{\ddagger}$	$N_{G,S}^*$	Abe*	$P_{G,S}^*$	$P_{\text{lit}}$	Ref.
(This Work)	(DR3)		(J2016)	(J2016)	[mag]	[K]	[ $M_{\odot}$ ]	[pc]					( $G$ )	( $G$ )			[hr]	[hr]			
Likely Spot	2216598405463898112	WD J15432.26+634154.11	328.634861	63.698414	18.9	0.997	16590.0	1.03	201.3	WD	0.4	.38	542.0	-0.205	0.131			1.01	7.383116		
Likely Spot	6613841171565998848	WD J221482.56+3433.98	333.719762	17.1	0.994	7670.0	0.75	53.9	WD	0.515	.42		0.22	0.068	42.0						
Known Spot	231557668254740.216	WD J003512.98+125088.84	8.809456	-12.419793	16.9	0.993	8440.0	0.81	DAte	52.7	WD	0.627	.26	623.0	-0.107	0.041				1.21048333	47
Known Spot	461361295121823104	WD J031715.85+853225.56	49.511809	-85.540486	14.8	1.0	26460.0	1.27	DAH	29.4	WD	0.614	.46		-0.146	0.136	46.0	0.607	0.6268161	0.20138889	48
Known Spot	55115326105246208	WD J041246.85+754942.26	63.192633	75.828522	15.8	0.991	8600.0	0.76	DAte	35.0	WD	0.525	.51	418.0	0.249	0.037	52.0	0.933	2.2891	2.2891	49,50
Known Spot	501240778459455872	WD J054342.93+7075.40	83.637543	77.131959	16.5	0.995	10670.0	0.84		60.7				48	0.176	0.074	48.0	0.909	0.7234655	0.72347	51
Known Spot	1020641700210987520	WD J098125.94+530936.72	147.858533	15.3	0.983	126070.0	0.78	DA	314.7	WD	0.596	.54	397.0	-0.461	0.099			82.8			52
Known Spot	368246912283597056	WD J125230.93-023417.72	193.129111	-2.571767	17.5	0.992	7746.0	0.56	DAte	77.7	WD	0.555	.58		-0.362	0.054			0.888132778		
Known Spot	4235280071072332672	WD J195629.23-010232.67	299.11983	-1.045547	13.6	0.994	7790.0	0.7	DA	11.6	WD	1.0	.36					34.60319444	54,55		
Known Spot	1748833236082347136	WD J202932.51+4070.07.70	307.385483	7.018813	16.6	0.943	63100.0	0.52	DO	522.1	WD	0.294	.45	183.0	-0.08	0.038			6.96	56,57	

**References**—<sup>†</sup> WD J Name,  $P_{\text{WD}}$  and atmospheric parameters determined from H-atmosphere fits of Gentile Fusillo et al. (2021). Spectral type information collected from the Montreal White Dwarf Database and SiMBAD. All Gaia information arises from DR2 (Gaia Collaboration et al. 2022c). <sup>‡</sup> The best classification (Class) and classification score (Score) arise from the variability classification table in DR3 (v2.1; isum). <sup>\*\*</sup> Information from Zwicky Transient Facility, including the number of per-FoV transits used in the short-period analysis ( $N_G, S$ ), the mean of per-FoV Abbe values (Abe $_{\text{av}}$ ), and the hypothesized timescale of variability ( $P_G, S$ ). <sup>\*</sup> Information for any objects flagged as short-timescale sources, such as the number of FoV transits used in the short-period analysis (v2.1; isum). <sup>\*</sup> Information from the short-timescale sources table in DR3 (v2.1). Literature periods have been collected from (1) Kepler et al. (2016); (2) Koester et al. (2020); (3) Kleiman et al. (2020); (4) Tremblay et al. (2020); (5) Ren et al. (2023); (6) Liebert et al. (1980); (7) Dreizler et al. (1995); (8) Kepler et al. (2015); (9) Ren et al. (2023); (10) Barnes et al. (2013); (11) Michaelian (2008); (12) Kepler et al. (2015); (13) Ren et al. (2013); (14) Howell et al. (2023); (15) Raditt et al. (2017); (16) Drake et al. (2010); (17) Eikenberry et al. (2016); (18) Kilic et al. (2016); (19) Ren et al. (2023); (20) Kowalski et al. (2022); (21) Boura et al. (2016); (22) Parsons et al. (2015); (23) Drake et al. (2010); (24) Boura et al. (2016); (25) Marsh & Duck (1996); (26) Drake et al. (2017); (27) Kowalski et al. (2016); (28) Kao et al. (1999); (29) Roberts-Munsigas et al. (2010); (30) Drake et al. (2010); (31) Boura et al. (1999); (32) Walter (1998); (33) Huppenkothen et al. (2017); (34) Rea et al. (2017); (35) Guidry et al. (2012); (36) Kepler (1984); (37) Fontaine et al. (1980); (38) Romero et al. (2023); (39) Kilic et al. (1997); (40) Ferrario et al. (2001); (41) Raditt et al. (2001); (42) Kong et al. (2017); (43) Eisenstein et al. (2019); (44) Kawka & Verner (2012); (45) Kleiman et al. (2013); (46) Ren et al. (2023); (47) Reding et al. (2023); (48) Ferrario et al. (1997); (49) Walter et al. (2009); (50) Koester et al. (2001); (51) Dreizler et al. (2020); (52) Werner et al. (2019); (53) Reding et al. (2020); (54) Brinkworth et al. (2020); (55) Maxted et al. (2005); (56) Brinkworth et al. (2020); (57) Dreizler et al. (1995).

Most variables are categorized by their periods of variability (from 100 – 1500 s for pulsating white dwarfs, to minutes to days for spotted white dwarfs), as well as their position in the color-magnitude diagram (e.g., CVs are composed of a composite spectra mixing some fraction of a white dwarf, main-sequence star, and accretion disk, and are considerably over-luminous to an isolated white dwarf). Using the color-magnitude position along with any periods constrained from the survey light curves allows us to suggest likely classifications for the subset of objects in this manuscript; we will present full classification of all 1333 objects in a future publication.

We devote our attention here to objects where at least one Gaia light curve successfully identifies the period of variability of a candidate white dwarf. We consider Gaia to successfully recover a period if the Gaia-*G* periodogram has its highest peak matching (to within 0.05  $\mu$ Hz) the highest peak of an independent ZTF and/or TESS periodogram, or an independent Gaia bandpass light curve.

Regardless of its significance (we discuss further in Section 5), we use the highest-amplitude of the periodogram of the available Gaia, ZTF, and TESS datasets as an initial guess for a linear-least-squares (LLS) fit of a sinusoid to the data using the Python package lmfit (Newville et al. 2016). This process returns the best-fit period, amplitude, and phase of a single sinusoid to the light curve, as well as associated uncertainties. All reported periods in the main text of this manuscript are the LLS fits of the Gaia DR3 *G*-band photometry.

In total we find 105 candidate white dwarfs which have photometric variability periods that can be correctly measured from their Gaia DR3 light curve independently. Of these 105 objects, 72 have data from ZTF and 65 have data from TESS (including 32 with both ZTF and TESS data). Based on our classification (see Section 4), we show where these 105 objects sit in the Gaia color-magnitude diagram in Figure 1. Because binary systems and objects with cool spots both show sinusoidal variability, we use mass and temperature estimate fits to Gaia photometry by Gentile Fusillo et al. (2021) (listed in Table 2) to distinguish between these objects. We classify candidate white dwarfs with an effective

temperature of  $> 31,000$  K or a photometrically determined mass  $< 0.525 M_{\odot}$  (which cannot have formed as single-stars within a Hubble time) as binaries; all other sinusoidally variable white dwarfs are classified as rotationally modulated spots. Since not all spotted white dwarfs are strongly magnetic (e.g., Hermes et al. 2017b), the only way to absolutely distinguish between a spot or binary is to use follow-up spectroscopy to search for radial-velocity variability.

Previous spectroscopy exists for just 36 of our 105 targets. Our photometric classifications lacking spectroscopic constraints will suffer some ambiguity. For example, WD J202932.51+070107.70 is hotter than 31,000 K and exhibits absorption from ultra-highly excited metals, but is likely variable due to a magnetic spot (Reindl et al. 2021). Similarly, the  $> 100,000$  K white dwarf WD J095125.94+530930.72 is likely spotted, based on a lack of radial-velocity variation (Werner et al. 2019). Still, classifying as binaries the sinusoidal variables with  $T_{\text{eff}} > 31,000$  K or  $M_{\text{WD}} < 0.525 M_{\odot}$  will be appropriate for the vast majority of our objects.

#### 4. CLASSIFIED WHITE DWARF VARIABLES

We attempt to classify the origin of the variability for the 105 candidate variable white dwarfs where we can measure a coherent, sinusoidal variability period from the Gaia light curves that matches a period detected in an independent dataset. Initially we inspect the Gaia DR3 machine learning output classifier (GaiaDR3Class), which is available for 62/105 objects. In most cases, however, this classifier simply says WD, revealing little about the specific nature of these objects.

We instead classify all objects based on variability period and position in the Gaia color-magnitude diagram, informed by past white dwarf variability studies (Hermes et al. 2017a; Reding et al. 2018). All discovery literature on our sources is collected in Table 2, and our full classification and variability information is collected in Table 3. Table 1 provides a summary of the overall sample and our analyzed sub-sample referenced in this manuscript.

**Table 3.** New variability information determined for the 105 white dwarfs in this study with significant variability measured from their Gaia DR3 light curve.

Class	WD J Name <sup>†</sup>	$P_{\text{G}, \text{DR3}}$	$\sigma P_{\text{G}, \text{DR3}}$	$A_{\text{G}}$	$\sigma A_{\text{G}}$	$t_{\text{min,G}}$	$\sigma t_{\text{min,G}}$	Match	$P_{\text{ZTF}}$	$\sigma P_{\text{ZTF}}$	$A_{\text{ZTF}}$	$\sigma A_{\text{ZTF}}$	$P_{\text{TESS}}$	$\sigma P_{\text{TESS}}$	$A_{\text{TESS}}$	$\sigma A_{\text{TESS}}$	Rev.	Std. Rev.	[d]	[d]	False Alarm
(This Work)		[hr]	[hr]	[Rel. Amp.]	[Rel. Amp.]	[d]	[d]		[hr]	[hr]	[hr]	[hr]	[hr]	[hr]	[hr]	[hr]			[%]		
Likely Binary	WD J003213.13+164934.78	21.771792	0.00451811	0.0053	0.004	56890.44	1.73	ZTF, TESS	21.886956	0.05957178	0.6484	0.3454	19.02039	0.38635659	0.0036	0.0014	52.9	43.2	0.7		
Likely Binary	WD J003449.86-31.2952.69	2.314931	0.00036725	0.0357	0.0157	56870.52	0.08	TESS	8.373517	0.00404841	0.2803	0.1418	8.362556	0.00191441	0.0035	0.0015	50.5	40.0	<0.1		
Likely Binary	WD J011053.06+604831.03	8.357258	0.00766065	0.007	0.006	56897.32	0.57	TESS	119.6655	0.4181806	0.7473	0.1757	122.246833	47.54794444	0.0042	0.0032	35.3	22.1	<0.1		
Likely Binary	WD J012828.99-385436.63	11.8.136167	0.46444972	0.0155	0.0041	56909.06	2.68	ZTF	2.056135	0.00019699	0.6549	0.2721	2.025781	0.009804038	0.0096	0.0036	56.7	47.6	24.9		
Likely Binary	WD J013148.02-055900.14	2.055886	0.00033342	0.01	0.0055	56897.97	0.11	TESS	12.770364	0.0103218	0.3655	0.1777	23.463694	0.75380139	0.0048	0.0026	38.8	30.6	27.5 <0.1		
Likely Binary	WD J022704.34+591502.04	12.736292	0.0122765	0.0073	0.0034	56898.86	0.59	ZTF	8.618753	0.4500	0.0	0.5263	8.618753	0.75380139	0.0048	0.0026	30.6	8.3	4.6		
Likely Binary	WD J032205.10-472106.46	24.768553	0.02279821	0.0393	0.0129	56912.94	0.43	TESS	26.073331	0.11561044	0.1405	0.1963	26.073331	0.75380139	0.0048	0.0026	65.6	57.7	28.8		
Likely Binary	WD J032803.02-265151.65	8.611367	0.00638363	0.0314	0.0211	56904.43	0.42	ZTF	4.0431	0.00155644	1.2607	0.6927	4.0431	0.00155644	1.2607	0.6927	51.2	43.8	5.2		
Likely Binary	WD J032902.63+390340.87	4.036247	0.00198667	0.0242	0.0159	56903.7	0.23	ZTF	1.794894	0.00033893	0.7248	0.6254	1.794894	0.00033893	0.7248	0.6254	39.3	29.8	<0.1		
Likely Binary	WD J03584.45-21.3813.74	1.794933	0.000233552	0.0227	0.0118	56914.03	0.09	ZTF	8.693579	0.11	TESS	2.871769	0.000595186	0.002	0.0019	35.9	13.1	15.9			
Likely Binary	WD J041033.37-585203.63	2.872539	0.00055393	0.0394	0.0189	56915.27	0.11	ZTF	2.434496	0.00043268	2.0772	0.7928	2.434496	0.00043268	2.0772	0.7928	50.4	46.0	21.9		
Likely Binary	WD J043103.75-041702.63	26.014614	0.06736786	0.0099	0.0049	56914.98	1.14	ZTF	26.073331	0.11561044	0.1405	0.1963	26.073331	0.75380139	0.0048	0.0023	43.2	37.5	1.1		
Likely Binary	WD J050433.01-21.3079.73	15.028869	0.02485904	0.0143	0.0107	56918.23	0.87	ZTF	14.956056	0.01491123	1.5712	0.9047	14.956056	0.75380139	0.0048	0.0023	36.6	23.7	4.4		
Likely Binary	WD J053632.07+123128.65	3.801928	0.00249101	0.0102	0.0126	56912.42	0.46	ZTF, TESS	3.799925	0.00054618	0.3572	0.2873	3.840864	0.03100203	0.002	0.0023	47.9	47.7	<0.1		
Likely Binary	WD J061234.26-191111.75	2.224975	0.00058326	0.0143	0.0134	56919.44	0.16	ZTF	2.225262	0.00038728	1.3633	0.9595	2.225262	0.00038728	1.3633	0.9595	36.7	27.1	1		
Likely Binary	WD J061815.27-512305.52	9.674728	0.00529894	0.0112	0.0094	56932.46	0.31	TESS	6.041864	0.00277571	0.5138	0.3596	6.041864	0.00072595	0.0091	0.0015	35.0	11.1	28.6		
Likely Binary	WD J064316.01+30312.78	6.036606	0.00212576	0.0224	0.0097	56918.12	0.24	ZTF, TESS	6.041864	0.00277571	0.5138	0.3596	6.041864	0.00072595	0.0091	0.0015	60.1	49.8	22.3		
Likely Binary	WD J064573.57-493756.16	7.011806	0.0108999	0.0142	0.0172	56996.71	0.67	Gaia BP	8.279997	0.00263236	4.3029	1.709	8.279997	0.000170344	0.005	0.0015	32.5	10.0	<0.1		
Likely Binary	WD J064802.27-634629.90	3.775729	0.00142423	0.0166	0.0146	56931.78	0.2	TESS	8.956211	0.00547992	0.1324	0.0848	8.956211	0.00529426	0.0002	0.0001	34.9	10.6	<0.1		
Likely Binary	WD J070647.52+61.3550.31	8.965739	0.00730369	0.0044	0.0021	56904.96	0.45	ZTF, TESS	2.714582	0.00135891	1.2807	1.4401	2.714582	0.39214361	0.0033	0.0097	44.7	33.5	7		
Likely Binary	WD J071246.74-564408.41	2.715027	0.00056963	0.0218	0.012	56907.27	0.14	ZTF	5.309414	0.00956094	0.1098	0.3165	5.313603	0.13041861	0.0	0.0013	51.8	44.8	3.6		
Likely Binary	WD J07121.39-595737.01	3.150798	0.00316432	0.0104	0.0106	56906.67	0.33	ZTF, TESS	8.279997	0.00263236	4.3029	1.709	8.279997	0.000170344	0.005	0.0013	46.9	37.6	33.7		
Likely Binary	WD J074316.04-493756.68	8.310972	0.00983921	0.0109	0.0187	56909.69	0.64	ZTF	5.416497	0.02826309	0.0445	0.02826309	5.416497	0.02826309	0.0445	0.0026	33.9	11.8	9		
Likely Binary	WD J079240.38-742331.37	5.449139	0.00180344	0.0101	0.0045	56931.38	0.21	ZTF, TESS	29.178917	0.03566194	1.0295	0.4407	42.434667	4.53270833	0.0099	0.0049	49.6	44.6	0.5		
Likely Binary	WD J079417.48-20e001641.72	29.146361	0.08106744	0.0119	0.0097	56962.01	1.71	TESS	2.744139	0.000240416	0.780175	0.2780175	2.744139	0.000240416	0.780175	0.2780175	36.4	20.0	<0.1		
Likely Binary	WD J093611.12-340059.16	20.793195	0.03595738	0.0067	0.0043	56965.69	0.13	TESS	2.535475	0.00043236	0.5741	0.3772	2.535475	0.00034043	0.0023	0.0013	57.0	50.2	17.6		
Likely Binary	WD J103121.39-595737.01	3.150798	0.00316432	0.0124	0.0185	56959.73	0.13	ZTF, TESS	432.56336	0.294925	0.0722	0.0772	432.56336	0.294925	0.0722	0.0772	38.1	19.1	<0.1		
Likely Binary	WD J1064802.27-634629.90	8.229394	0.00471778	0.0	0.0001	56974.03	0.64	TESS	1.83	0.5688.84	0.0774	0.0774	1.83	0.5688.84	0.0774	0.0774	36.1	31.5	5.9		
Likely Binary	WD J110417.48-20e001641.50	29.047667	0.094925	0.0272	0.0174	56987.85	0.45	TESS	16.985225	0.135344694	0.0	0.0	16.985225	0.135344694	0.0	0.0	45.4	30.1	12.8*		
Likely Binary	WD J112355.12-40e01641.63	16.972742	0.01447909	0.0288	0.0131	56987.98	0.13	ZTF	2.744139	0.000240416	0.780175	0.2780175	2.744139	0.000240416	0.780175	0.2780175	36.0	11.9	3.1		
Likely Binary	WD J113117.73	13.311775	0.03923664	0.0008	0.0068	56891.91	1.75	Gaia BP, Gaia RP	23.246072	0.01754755	0.01754755	0.0206	23.246072	0.01754755	0.0206	0.0051	33.5	14.0	9.3		
Likely Binary	WD J11622.61-545907.30	2.576151	0.000503299	0.0664	0.035	56894.91	0.11	Gaia BP, Gaia RP	0.956609	0.00014681	4.9308	5.1684	0.956609	0.00014681	4.9308	5.1684	34.1	17.6	0.1		
Likely Binary	WD J12395.40-834707.51	0.956676	0.00035594	0.0388	0.0262	56895.88	0.19	ZTF	21.082511	0.03706747	0.9748	0.9013	21.082511	0.03706747	0.9748	0.9013	47.2	22.8	7.4		
Likely Binary	WD J125007.11-20e3632.29	21.147906	0.02900806	0.0345	0.0268	56896.21	0.91	TESS	0.5	0.0708	56900.83	0.1249	0.7035	0.0708	0.1249	0.7035	62.8	50.7	12		
Likely Binary	WD J135323.92-085645.42	2.744149	0.00026954	0.0132	0.0132	56901.83	0.45	ZTF, TESS	3.4503	0.0066051	0.6072	0.3348	3.4503	0.0066051	0.6072	0.3348	31.9	16.9	<0.1		
Likely Binary	WD J140330.89-671255.16	3.443786	0.000139008	0.0168	0.0122	56897.06	0.24	ZTF	0.0772	0.01444292	0.7476	0.2314	0.0772	0.01444292	0.7476	0.2314	30.5	16.8	<0.1		
Likely Binary	WD J144007.60-31.5413.02	23.243372	0.04633281	0.0135	0.0083	56913.96	1.1	ZTF, TESS	2.377583	0.0000173	1.8722	1.8722	2.377583	0.0000173	1.8722	1.8722	37.8	13.4	9.3		
Likely Binary	WD J145623.30-793654.99	4.819789	0.0016514	0.0221	0.0159	56898.87	0.22	Gaia BP	0.956609	0.00014681	4.9308	5.1684	0.956609	0.00014681	4.9308	5.1684	32.5	10.2	<0.1		
Likely Binary	WD J145817.91-651024.94	3.677164	0.00275866	0.004	0.0062	56900.11	0.5	Gaia BP	0.956609	0.00014681	4.9308	5.1684	0.956609	0.00014681	4.9308	5.1684	31.9	16.9	<0.1		
Likely Binary	WD J153028.82-24e01748.48	21.206987	0.02246878	0.0186	0.007	56904.12	0.54	TESS	2.744139	0.000240416	0.780175	0.2780175	2.744139	0.000240416	0.780175	0.2780175	32.5	8.7	<0.1		
Likely Binary	WD J154012.60-290828.96	2.377268	0.00026954	0.0467	0.0179	56914.48	0.07	ZTF	4.744139	0.000240416	0.780175	0.2780175	4.744139	0.000240416	0.780175	0.2780175	30.5	16.8	<0.1		
Likely Binary	WD J18124.55-465721.46	3.739088	0.0001654	0.0221	0.0159	56930.63	0.14	ZTF	3.737569	0.00010204	0.374	0.2643	3.737569	0.00010204	0.374	0.2643	37.8	13.4			

**Table 3 (continued)**

Class	WD Name <sup>†</sup>	$P_{G,DR3}$	$\sigma P_{G,DR3}$	$A_G$	$\sigma A_G$	$t_{\min,G}$	$\sigma t_{\min}$	Match	$P_{ZTF}$	$\sigma P_{ZTF}$	$A_{ZTF}$	$\sigma A_{ZTF}$	$P_{TESS}$	$\sigma P_{TESS}$	$A_{TESS}$	$\sigma A_{TESS}$	Rev.	Std. Rev.	False Alarm
(This Work)		[hr]	[hr]	[Rel. Amp.]	[Rel. Amp.]	[d]	[d]		[hr]	[hr]	[hr]	[hr]	[hr]	[hr]	[hr]	[d]	[d]	[%]	
Likely Binary	WD J109892.94+143534.17	7.188675	0.0166399	0.0029	0.0059	5.699227	1.04	ZTF	7.191394	0.00177492	0.8598	0.3362	42.2	30.9	0.4			<0.1	
Likely Binary	WD J200937.02+165219.12	2.498782	0.00868119	0.0176	0.0127	5.6998577	0.15	ZTF	2.50491	0.00017069	2.4724	0.5959	2.547105	0.02237542	0.0085	0.0055	40.0	29.4	
Likely Binary	WD J202354.74+433512.12	5.324653	0.00283764	0.0192	0.0106	5.69904.84	0.28	TESS					5.302883	0.00018972	0.024	0.0072	31.7	9.4	2.4
Likely Binary	WD J202354.90+433513.67	15.2327	0.02066798	0.0214	0.0114	5.6914.23	0.69	TESS					16.172639	0.02935103	0.0278	0.0049	51.3	41.7	<0.1
Likely Binary	WD J202841.18e-325837.35	19.422681	0.02611342	0.0656	0.0348	5.6966.42	0.66	ZTF, TESS	19.616389	0.02075202	2.0971	1.0358	21.614186	0.15849081	0.0392	0.0392	32.7	12.6	<0.1
Likely Binary	WD J21010.17-452715.14	12.874175	0.01180351	0.0077	0.0031	5.6957.41	0.45	Gaia BP, Gaia RP	12.673865	0.005555556	0.0	0.0066	51.5	43.6	0.5				
Likely Binary	WD J210840.53e-554502.63	2.781769	0.00053615	0.0281	0.0141	5.6873.09	0.09	ZTF	2.78206	0.0006235	0.7013	0.5455	37.2	16.3	0.3				
Likely Binary	WD J211557.38e-364255.40	6.7535303	0.00451239	0.0125	0.0088	5.6965.93	0.36	ZTF	6.748281	0.00153208	1.049	0.3375	6.748281	0.00153208	0.0036	0.0024	57.0	50.1	32.1
Likely Binary	WD J213109.35e-364256.84	10.372323	0.0130606	0.0105	0.0079	5.6988.5	0.61	ZTF	10.412589	0.00143792	1.075	0.3873	10.412589	0.00143792	0.0036	0.0027	37.1	22.2	<0.1
Likely Binary	WD J213958.29+074126.17	6.250269	0.00316512	0.0244	0.0108	5.6983.85	0.25	ZTF	6.261194	0.00157262	1.4742	0.6431	6.261194	0.00157262	0.0036	0.0027	53.2	46.4	<0.1
Likely Binary	WD J221545.15e-503759.46	5.414369	0.00237553	0.0224	0.0144	5.6882.25	0.25	ZTF	5.431119	0.000513291	1.6915	1.2771	5.431119	0.000513291	0.0036	0.0027	35.7	13.0	12.2
Likely Binary	WD J224559.30e-201633.35	3.905189	0.00094466	0.0096	0.0051	5.6867.64	0.11	ZTF	3.906517	0.00084593	0.1878	0.0921	60.1	45.2	6.6				
Likely Binary	WD J224663.73-094833.48	19.326454	0.01023835	0.0452	0.0036	5.6958.88	0.31	TESS	19.837572	0.16538897	1.1215	0.5601	18.508856	0.11626889	0.036	0.0024	57.0	50.1	32.1
Likely Binary	WD J225206.39-274012.56	5.132572	0.0023864	0.0258	0.0159	5.6985.48	0.31	ZTF	5.133864	0.000253317	0.6989	0.6005	5.133864	0.000253317	0.0036	0.0027	58.8	51.9	4.6
Likely Binary	WD J230047.06e-125015.98	16.714308	0.02454316	0.0129	0.0007	5.6959.68	0.93	TESS	16.589397	0.01973398	0.0991	0.0436	16.554344	0.01973398	0.0057	0.0011	62.4	52.3	
Likely Binary	WD J232411.16e-653065.05	7.271892	0.00379897	0.0196	0.0099	5.6895.47	0.33	ZTF, TESS	7.303556	0.00047147	0.491	0.3447	7.314125	0.00047069	0.0021	0.0021	31.8	8.9	<0.1
Likely Binary	WD J233923.79-485350.19	2.529616	0.00074594	0.0091	0.0078	5.6912.48	0.14	TESS					2.521869	0.01775451	0.002	0.0021	36.4	27.2	<0.1
Likely Eclipsing Binary	WD J004502.55e-503408.46	6.883219	0.00192382	0.0772	0.0294	5.6927.53	0.16	ZTF	6.869319	0.00253022	1.1385	0.4951	6.869319	0.00253022	0.0036	0.0024	41.8	31.2	40.7
Likely Eclipsing Binary	WD J130905.43-470852.39	3.320388	0.00107816	0.0589	0.0493	5.6896.94	0.22	Gaia RP					5.26	38.5	27.5				
Likely Eclipsing Binary	WD J154008.28-392917.61	1.31965	0.001056547	0.0486	0.0276	5.6903.93	0.06	TESS					46.0	39.4	28.5				
Likely Eclipsing Binary	WD J202811.64e-505225.08	10.405553	0.000659212	0.0212	0.0081	5.6963.46	0.34	ZTF	10.36467	0.001144	0.3689	0.2038	10.36467	0.001144	0.0028	0.0017	32.7	13.7	1.8
Known Eclipsing Binary	WD J033524.64e-385529.70	4.861628	0.00057632	0.0082	0.0111	5.6895.07	0.84	ZTF	4.86289	0.001144	0.9914	0.4022	4.86289	0.001144	0.0028	0.0017	52.6	39.9	<0.1
Known Eclipsing Binary	WD J087487.18e-034255.35	1.561434	0.00047608	0.0307	0.0246	5.6956.65	0.14	ZTF	1.561681	0.0001148	2.6183	1.2482	1.561681	0.0001148	0.0036	0.0027	49.5	44.8	<0.1
Known Eclipsing Binary	WD J132518.18e-233808.02	4.678903	0.0018771	0.0127	0.0074	5.6886.94	0.25	ZTF	4.674961	0.0018441	0.6449	0.5285	4.674961	0.0018441	0.0036	0.0027	48.2	37.5	0.2
Known Eclipsing Binary	WD J071097.79e-740040.53	2.472226	0.00034023	0.0078	0.0032	5.6902.62	0.08	ZTF, TESS	2.474291	0.00035304	0.1626	0.0756	2.473012	0.00029588	0.0006	0.0003	33.1	14.5	21
Known Binary	WD J093017.97-252114.79	7.644542	0.00065031	0.0145	0.0063	5.6903.73	0.34	TESS	5.721197	0.00086724	0.598	0.2038	5.721197	0.00086724	0.0028	0.0017	33.5	17.1	<0.1
Known Binary	WD J153938.12-260653.84	5.721225	0.00053404	0.0032	0.0033	5.6914.25	0.5	TESS					5.721225	0.00023915	0.0028	0.0017	54.9	44.6	
Likely CV	WD J130017.86-325806.23	0.603127	9.41e-05	0.1924	0.2752	5.7021.15	0.08	Gaia BP, Gaia RP					5.7021.15	0.001148	0.0036	0.0006	33.9	17.1	3.7*
Known CV	WD J031411.32e-223542.92	1.349474	0.00016573	0.0242	0.0178	5.6912.08	0.07	TESS	5.7022.08	0.00015006	2.167	1.0267	5.7022.08	0.00015006	0.0099	0.0053	50.1	37.3	29.8
Known CV	WD J083843.35-282701.14	16.109283	0.02880356	0.0893	0.0609	5.6960.29	0.99	Gaia BP, Gaia RP	5.7023.07	0.000196275	0.3572	0.2035	5.7023.07	0.000196275	0.0099	0.0027	57.6	49.9	12.3
Likely DAV	WD J082924.77-163337.25	1.77e-06	0.009779	0.0079	0.0086	5.6959.48	0.01	ZTF	5.709723	6.9e-07	1.195	0.7069	5.709723	6.9e-07	0.003	0.0014	48.6	34.4	2.5
Likely DAV	WD J020322.04e-255851.90	25.724439	0.04730978	3.6e-07	0.004	5.6893.04	0.0	TESS					5.724439	0.001148	0.0018	0.0004	65.7	55.8	10.2
Known DAV	WD J095227.88e-280929.18	0.07111	7.6e-07	0.0036	0.0031	5.6901.42	0.01	ZTF	0.071112	3.3e-07	0.2168	0.1663	0.071111	3e-07	0.0009	0.0006	33.9	17.1	3.7*
Known DAV	WD J15823.88-585353.81	0.086112	5.8e-07	0.0079	0.0037	5.6898.17	0.38	TESS	0.086111	8.4e-07	0.086111	0.086111	0.086111	8.4e-07	0.0003	0.0003	37.9	22.1	28.9*
Likely Spot	WD J011157.12e-2313632.67	9.814925	0.010904233	0.0043	0.0043	5.6897.32	1.42	ZTF	9.821594	0.00612669	0.3733	0.2035	9.821594	0.00612669	0.0099	0.0027	57.6	49.9	
Likely Spot	WD J103832.02-195446.58	3.941892	0.00110964	0.0051	0.0053	5.6891.56	0.16	ZTF	3.943017	0.00196275	0.3572	0.2035	3.943017	0.00196275	0.0099	0.0027	43.4	35.1	<0.1
Likely Spot	WD J020322.04e-255851.90	25.724439	0.04730978	3.6e-07	0.004	5.6893.56	0.86	TESS					5.724439	0.001148	0.0018	0.0044	65.7	55.8	10.2
Likely Spot	WD J024235.52-820636.32	3.542838	0.00118396	0.0068	0.0049	5.6897.31	0.1	TESS	0.071112	3.3e-07	0.2168	0.1663	0.071111	3e-07	0.0009	0.0006	33.9	17.1	3.7*
Likely Spot	WD J052026.35e-38240.87	6.78556	0.00051865	0.0084	0.0093	5.6876.94	0.0	TESS	0.071112	3.3e-07	0.2168	0.1663	0.071111	3e-07	0.0009	0.0006	33.9	17.1	3.7*
Likely Spot	WD J024235.52-820636.32	3.542838	0.00118396	0.0068	0.0049	5.6876.94	0.0	TESS	0.071112	3.3e-07	0.2168	0.1663	0.071111	3e-07	0.0009	0.0006	33.9	17.1	3.7*
Likely Spot	WD J14441.00e-214338.33	4.459511	0.001264231	0.0043	0.0043	5.6878.2	3.13	ZTF	228.33778	2.97987222	0.508	0.2783	228.33778	2.97987222	0.0474	0.0027	11.0918	51.9	39.8
Likely Spot	WD J14441.00e-214338.33	4.459511	0.001264231	0.0043	0.0043	5.6878.2	3.13	ZTF	2.161886	0.00042694	1.6366	1.0268	2.161886	0.00042694	0.0036	0.0014	49.1	40.6	33.7
Likely Spot	WD J09012.89-394553.32	3.560872	0.00073476	0.0081	0.0028	5.6878.17	0.0	TESS	0.071112	3.3e-07	0.2168	0.1663	0.071111	3e-07	0.0009	0.0006	33.9	17.1	3.7*
Likely Spot	WD J115023.35e-35e03618.07	0.245574	0.00262-06	0.0118	0.0055	5.6878.2	0.0	TESS	0.071112	3.3e-07	0.2168	0.1663	0.071111	3e-07	0.0009	0.0006	33.9	17.1	3.7*
Likely Spot	WD J124740.10e-30307.41	225.656194	1.46535381	0.001264231	0.0043	5.6878.2	0.0	TESS	0.071112	3.3e-07	0.2168	0.1663	0.071111	3e-07	0.00				

**Table 3 (continued)**

Class	WD J Name <sup>†</sup>	$P_{\text{G,DR3}}$	$\sigma P_{\text{G,DR3}}$	$A_{\text{G}}$	$\sigma A_{\text{G}}$	$t_{\text{min,G}}$	$\sigma t_{\text{min}}$	Match	$P_{\text{ZTF}}$	$\sigma P_{\text{ZTF}}$	$A_{\text{ZTF}}$	$\sigma A_{\text{ZTF}}$	$P_{\text{TESS}}$	$\sigma P_{\text{TESS}}$	$A_{\text{TESS}}$	$\sigma A_{\text{TESS}}$	Rev.	Std. Rev.	False Alarm
(This Work)		[hr]	[hr]	[Rel. Amp.]	[Rel. Amp.]	[d]	[d]		[hr]	[hr]	[hr]	[Rel. Amp.]	[Rel. Amp.]	[hr]	[hr]	[d]	[d]	[%]	
Likely Spot	WD J215432.26-634154.11	0.934589	6.78e-05	0.0244	0.015	56892.59	0.04	ZTF	0.934499	5.65e-05	0.6797	0.4345	6.902656	0.13466103	0.0663	0.003	33.8	10.6	0.6
Likely Spot	WD J221432.26-314333.98	7.392242	0.00398888	0.0142	0.0071	56951.62	0.35	TESS	0.60499	1.93e-05	0.4396	0.2066	26.4897778	0.0	0.0	49.5	43.3	0.2	
Known Spot	WD J003512.88-12508.84	0.605106	6.89e-06	0.078	0.0054	56879.66		ZTF, TESS	0.201389	0.0003	0.0003	0.0003	65.5	51.2	0.0	0.0	25.3		
Known Spot	WD J031715.85-853225.56	0.201399	1.92e-06	0.0362	0.013	56897.19	0.01	TESS	0.0005979	0.0	0.0005979	0.0	32.5	8.8	<0.1	<0.1			
Known Spot	WD J041246.85-75492.26	0.344425	9.77e-06	0.0066	0.0036	56937.29	0.12	ZTF, TESS	0.34443	1.04e-05	0.2687	0.1765	0.344439	5.52e-06	0.0013	0.0006	33.1	14.6	4.2
Known Spot	WD J053432.35-70757.40	0.723311	7.13e-05	0.0076	0.0085	56900.79	0.06	ZTF, TESS	0.72323	16.2389444	0.0	0.0064	0.72334	0.0045125	0.0	0.0004	35.6	13.5	5.5*
Known Spot	WD J098125.94-530930.72	82.886	1.00760111	0.0132	0.0119	56918.71	6.77	ZTF, TESS	0.503975	0.7059	0.509	83.266694	0.14100106	0.0038	0.0007	36.4	25.6	<0.1	
Known Spot	WD J125230.93-023417.72	0.088057	0.00133891	0.0	0.0055	56890.23	7.57	TESS	0.088	5.57e-05	0.0023	0.0003	54.4	45.2	0.1	0.0003	44.0	41.6	<0.1
Known Spot	WD J195629.23-010232.67	34.8989417	0.07376844	0.016	0.0051	56917.58	1.05	TESS	0.047	0.04030639	0.0047	0.0003	48.0	41.6	<0.1	<0.1	36.0	36.0	13.8
Known Spot	WD J202932.51-070107.70	6.957214	0.0022029	0.0159	0.0045	56959.12	0.18	ZTF	6.971394	0.00149846	1.11	0.3097	7.140053	0.06677989	0.0173	0.0044	44.0	41.6	

References— \* Gaia BP ( $G_BP$ ) band used in analysis instead of Gaia G band. \*\* Gaia RP ( $G_RP$ ) band used instead of Gaia G band. Note that “Rev.” (revisit) is the average time between two Gaia detections of a source, and “Std. Rev.” is the standard deviation of this revisit time.

#### 4.1. Non-Eclipsing White Dwarf Binaries

Binary systems are often distinguishable from isolated white dwarfs because they are an unresolved pair of stars, making them over-luminous to single star cooling tracks, such as those shown in Figure 1. For this reason, over-luminous objects with sinusoidal variability that have an effective temperature exceeding 31,000 K as determined by the hydrogen-rich-atmosphere fits from Gentile Fusillo et al. (2021) or a photometrically determined mass  $< 0.525 M_{\odot}$  are categorized as binary systems. Objects without mass determinations from Gentile Fusillo et al. (2021) are likely over-luminous and also classified as binaries. Typical values for orbital periods of binary systems with a white dwarf paired with an M dwarf have been studied by Nekot Gómez-Morán et al. (2011), where SDSS data showed that post common envelope binaries containing a white dwarf and main sequence star have orbital periods ranging from 1.9 hr to 103.2 hr, with an average of approximately 10.3 hr.

We find 72 likely variable binaries in our sample, including seven eclipsing binaries (Section 4.3), with orbital periods ranging from 0.957 hr to 29.366 hr, with a mean of approximately 8.411 hr and a standard deviation of approximately 7.417 hr, consistent with the Nekot Gómez-Morán et al. (2011) distribution.

Three representative examples of variable binaries are shown in Figure 2. The first object (WD J153938.12+270605.84,  $G = 16.6$  mag) is a known DA+dM system with an orbital period of  $5.72120 \pm 0.00087$  hr measured from the Palomar Transient Factory (PTF, Kao et al. 2016). We measure from Gaia DR3 photometry only  $P_{\text{orb}} = 5.7213 \pm 0.0053$  hr, agreeing with the PTF measurement to within our estimated uncertainty. The second object (WD J041033.37–585203.63,  $G = 17.6$  mag) is a newly discovered binary system with a sinusoidal pattern in both the Gaia  $G$  and TESS bands with a Gaia  $G$  band period of  $2.87254 \pm 0.00054$  hr. The higher amplitude from the redder TESS data is indicative of flux reprocessing from a reflection-effect binary, though no spectroscopy exists for this target. Finally, WD J200937.02+165219.12 ( $G = 16.8$  mag) is also likely a new reflection-effect binary with an orbital period of  $2.49878 \pm 0.00086$  hr.

The shortest-period, likely detached new binary in our sample is WD J123955.40+834707.51 ( $G = 20.0$  mag), which shows significant variability in ZTF at  $0.95661 \pm 0.00015$  hr that is also seen in the Gaia  $G$ -band light curve at an amplitude exceeding 40%. No spectroscopy exists of this target, which has a position in the Gaia CMD consistent with a 7020 K,  $0.27 M_{\odot}$  white dwarf, suggesting it might be a new WD+WD binary containing at least one ELM white dwarf (e.g., Brown et al. 2022).

#### 4.2. Periodicities in Known Cataclysmic Variables

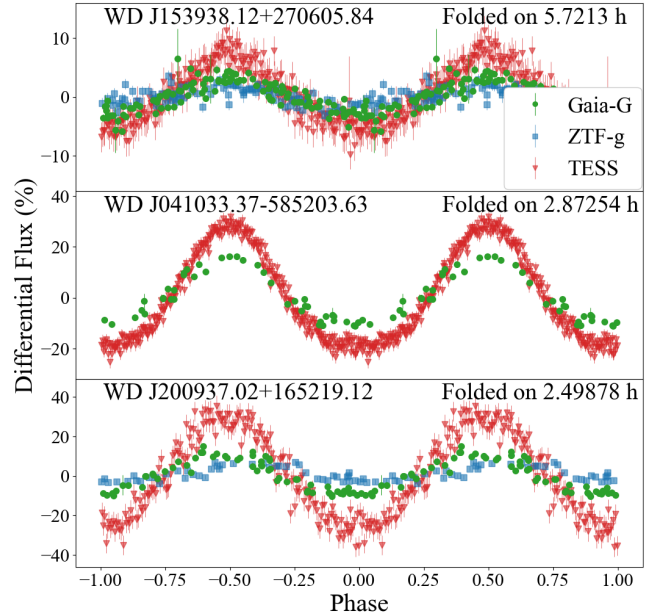


**Figure 2.** Phase-folded light curves of three representative variable white dwarfs from binarity, revealing orbital periods of 5.725 hr, 2.873 hr, and 2.500 hr, respectively. All folded light curves (ZTF  $g$  in blue, Gaia  $G$  in green, and TESS photometry in red) are phased to the same ephemeris. ZTF  $g$  and TESS data are grouped into 151 bins for each light curve. The larger amplitudes at redder wavelengths in these systems indicates they are all likely reflection-effect binaries of a cool main-sequence star reprocessing flux from a nearby hot white dwarf.

There are also likely some binaries that are not detached in our sample. CVs are a class of accreting white dwarf binaries, and are often eruptive variables that show large brightening events from dwarf novae and other outbursts (Szkody et al. 2020, 2021). We have not intended to search for new CVs among the 1333 high-confidence white dwarfs, which has been the focus of previous work on Gaia light curves using eruptions and outbursts (e.g., Gaia Collaboration et al. 2019). However, we have identified coherent periods in three objects classified as CVs in the literature.

WD J083843.35–282701.14 ( $G = 17.6$  mag) is a known CV (Halpern et al. 2017; Rea et al. 2017) for which we find a new potential period of variability of  $16.109 \pm 0.029$  hr. This period differs slightly from the approximately 15-hr period of flux variability interpreted as the beat period between the orbital and spin periods (Rea et al. 2017), as well as the  $14.7 \pm 1.2$  hr period of X-ray modulations observed by Halpern et al. (2017). WD J031413.25–223542.92 ( $G = 18.2$  mag) was studied by Warner (1980) and Bond et al. (1979). The Gaia DR3 data show a significant periodicity at  $1.34947 \pm 0.00017$  hr, which is in close agreement with both studies.

Finally, WD J130017.86–325805.23 ( $G = 20.3$  mag), is a CV candidate that has undergone at least two measured

outbursts detected in CRTS (Drake et al. 2014). We lack TESS or ZTF coverage for this faint southern object, but all three Gaia band-passes have their highest periodogram peak at 2171.36 s (36.2 min). The amplitude of the signal exceeds 80% in all Gaia band-passes. Such large-amplitude periodic variations are not commonly observed as spurious signals in Gaia DR3 at such short periods (Holl et al. 2023), though we cannot independently rule out an instrumental origin for this 36.2-min variability. We strongly encourage follow-up of this faint southern target.

#### 4.3. Eclipsing White Dwarf Binaries

Eclipsing binaries often display near-total flux dropouts in randomly sampled light curves (Parsons et al. 2013), as the fainter companion passes in front of the brighter member. These eclipses should occur at exactly the same phase in a folded light curve, manifesting as stable, repeated photometric variability. The seven known and likely eclipsing systems are shown in Figure 3.

The top panels in Figure 3 detail three previously known eclipsing white dwarf binaries, in order of orbital period. WD J085746.18+034255.35 ( $G = 18.3$  mag) is a known eclipsing WD+dM with a measured orbital period of 1.562317 hr by the Catalina Sky Survey (CSS, Parsons et al. 2015), which is consistent with our measurement from Gaia DR3 photometry of 1.562316(17) hr. This object shows both ZTF and Gaia dropouts, notable since the Gaia DR3 light curves have a reasonably aggressive outlier rejection (Eyer et al. 2023). WD J132518.18+233808.02 ( $G = 18.2$  mag) is also a known eclipsing DA+dM binary with an orbital period of 4.679 hr measured by CSS (Drake et al. 2010; Parsons et al. 2015) consistent with our measurement from Gaia DR3 photometry of 4.67901(39) hr. The lack of in-eclipse data from Gaia is likely related to outlier rejection of the Gaia photometry<sup>1</sup>. WD J003352.64+385529.70 ( $G = 18.3$  mag) was identified by Kosakowski et al. (2022) to have a strong 4.86-hr signal in ZTF, and has all the hallmarks of a WD+dM eclipsing binary, especially featuring ZTF dropouts in both the  $g$ - and  $r$ -bands when folded on a period of 4.86465(31) hr. These dropouts align in phase space and show a decrease in amplitude of nearly 100%.

Our analysis identifies four new candidate eclipsing binaries. Most compact is WD J154008.28–392917.61, showing multiple low Gaia points when folded on the TESS-determined period of 1.319(13) hr. We detail follow-up observations of this source in Section 4.3.1 and Figure 4.

WD J130905.43–470852.39 ( $G = 18.3$  mag) may be an eclipsing binary, having only Gaia light curves to analyze. When folded on a period of 3.32265(44) hr, the source shows dropouts in both the  $G$  and  $G_{RP}$  bands with small uncer-

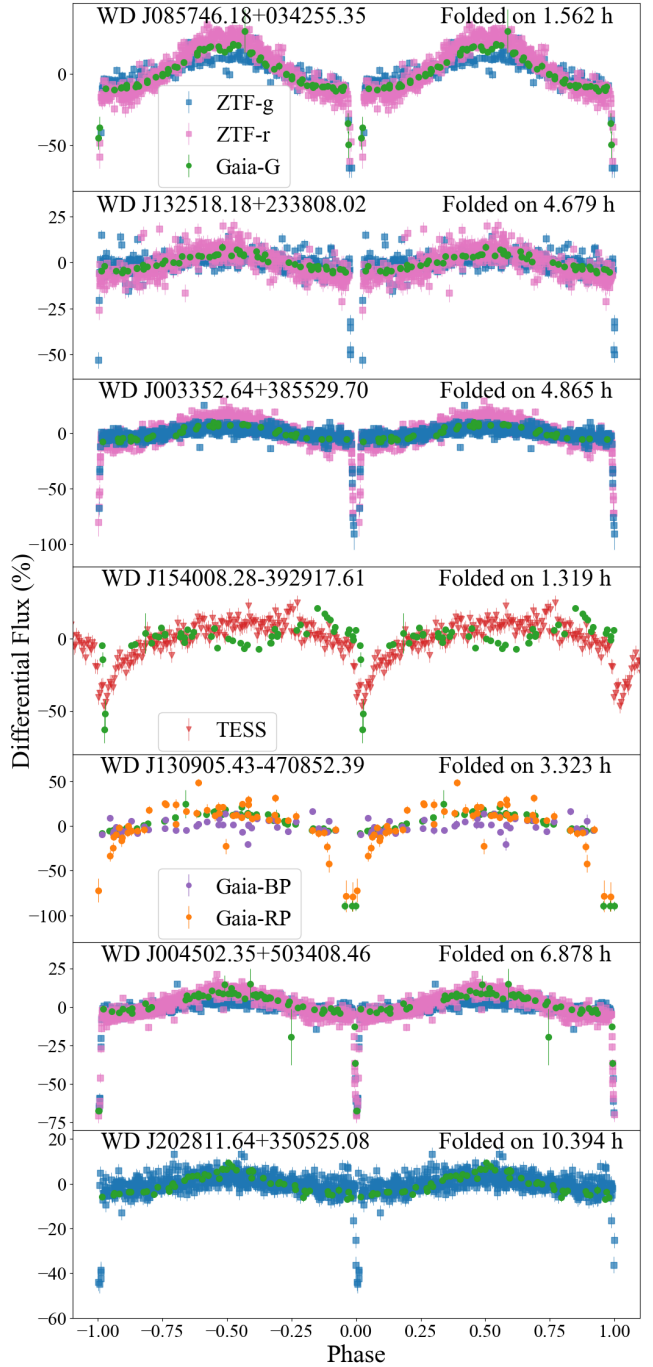


**Figure 3.** Following the same convention as Figure 2, we show phase-folded light curves of seven eclipsing binaries detected from their Gaia DR3 light curves. In this figure, ZTF and Gaia data are not binned, but TESS data are grouped into 251 bins. The first three systems are previously published eclipsing binaries containing a white dwarf (Drake et al. 2010; Parsons et al. 2015; Kosakowski et al. 2022). Four systems are newly discovered eclipsing binaries containing a white dwarf, including a new 1.3-hr eclipsing CV (WD J154008.28–392917.61, further detailed in Section 4.3.1 and Figure 4). With only sparse Gaia DR3 data, we do not claim to confirm binarity in WD J154008.28–392917.61, but include it as an interesting candidate.

<sup>1</sup> Gaia DR3 Documentation Section 5.1.4: Photometric Calibration

tainties leading us to believe that these are genuine eclipses. Photometric fits to the Gaia CMD suggest this system has an extremely low-mass ( $<0.16 M_{\odot}$ ), 11040 K white dwarf with a high probability of being a white dwarf ( $P_{\text{WD}} = 0.91$ , Gentile Fusillo et al. 2021). With only sparse Gaia DR3 data and possibly long transit durations, we cannot confirm this system as eclipsing yet, but encourage further follow-up.

We are far more confident in the fidelity of the final two systems shown in Figure 3. WD J004502.35+503408.46 ( $G = 17.6$  mag) is over-luminous to the isolated white dwarf position in the Gaia CMD (suggesting binarity) and features ZTF and Gaia dropouts suggesting an orbital period of 6.87794(72) hr. WD J202811.64+350525.08 ( $G = 17.9$  mag), is also over-luminous and features ZTF dropouts when folded on a period of 10.3937(17) hr. There is also a strong Gaia- $G$  sinusoidal pattern that aligns with the ZTF data with a minimum in the time of transit.

#### 4.3.1. Follow-Up of a New Eclipsing CV

We obtained follow-up time-series photometry and spectroscopy for our most compact new eclipsing system (WD J154008.28–392917.61), located in the southern hemisphere ( $G = 17.3$  mag).

We obtained high-speed time-series photometry using the ULTRACAM instrument (Dhillon et al. 2007) mounted on the 3.6-meter New Technology Telescope (NTT) telescope at the La Silla Observatory in Chile. This camera obtains simultaneous three-channel photometry with frame-transfer detectors; we used high-throughput Super-SDSS  $usgsrs$  filters (Dhillon et al. 2021). We observed WD J154008.28–392917.61 over two consecutive nights, analysing here only the SDSS- $g_s$  data. We collected 9.0-s exposures on UT date 2023 March 16 with an average seeing of 0.8 arcsec. We collected 4.5-s exposures on UT date 2023 Mar 17 with an average seeing of 0.7 arcsec. All ULTRACAM data were bias-subtracted and flat-field corrected using the HiPERCAM pipeline<sup>2</sup>.

We also obtained follow-up spectroscopy of this system using the Goodman spectrograph (Clemens et al. 2004) mounted on the 4.1-meter SOAR Telescope in Chile. We collected eleven 10 min spectra using the 400-line grating with a 1-arcsec slit and the M1 grating setup on UT date 2023 May 24, yielding a resolution of roughly 4.4 Å. We extracted the data using the pypeit data reduction pipeline (Prochaska et al. 2020), and flux calibrated using the standard star EG 274.

We captured two primary eclipses with ULTRACAM, shown in the top two panels of Figure 4. Fitting the mid-time of the eclipses with a Gaussian bounded by when the flux decreases below –20%, we find that the pri-

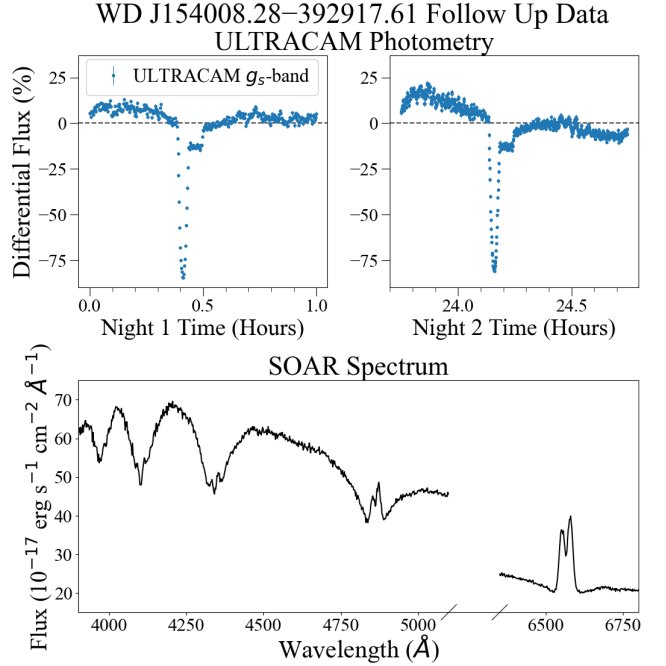


**Figure 4.** Follow up data for WD J154008.28–392917.61 reveals deep primary eclipses in the two top panels. Follow-up spectroscopy (note the broken x-axis) confirms this is a 68.365-min CV, likely descending from a previously detached white dwarf + brown dwarf post-common-envelope binary (e.g., Littlefair et al. 2007).

mary eclipses occur at  $\text{BJD}_{\text{TDB}} = 2460019.8887179(17)$  and  $2460020.8778468(11)$ , separated by 18 cycles of our TESS-determined main periodicity of 1.319(13) hr. There is considerable out-of-transit variability, including an extended feature from a bright spot on the white dwarf, seen in many eclipsing CVs (e.g., Savoury et al. 2011; McAllister et al. 2019).

Our coadded spectrum in the bottom panel of Figure 4 confirms this is an accreting white dwarf binary. Broad Balmer-line absorption from the white dwarf is visible, along with strong emission features from accretion, especially dominant at H $\alpha$ . Our spectrum is not high-enough resolution to attempt a radial-velocity fit. We do not observe Zeeman splitting at the Balmer lines, though our limits are weak given the strong emission in the line cores.

A purported orbital period of 68.365 min is well below the CV period minimum of roughly 80 min, after which convective donor stars expand on further mass loss (Patterson 1984; Knigge et al. 2011; Kalomeni et al. 2016; McAllister et al. 2019). However, the full photometric phase coverage from TESS shown in Figure 3 reveals this is the correct period of recurrent variability. This makes WD J154008.28–392917.61 among the shortest-period CVs known, similar to the 66.61-min CV SDSS J150722.30+523039.8 (Littlefair et al. 2007). These ultracompact CVs are likely descended from a previously de-

<sup>2</sup> <https://github.com/HiperCam/hipercam>

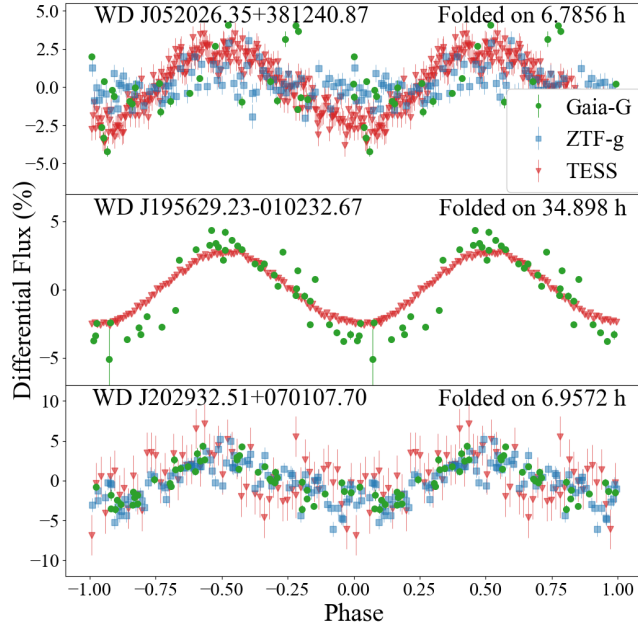


**Figure 5.** Following the same convention as Figure 2, we show phase-folded light curves of three magnetic spotted white dwarfs. ZTF-*g* and TESS data are grouped into 151 phase bins, whereas the Gaia data are not binned.

tached white dwarf + brown dwarf binary. It is also possible the system descended from a low-metallicity, significantly evolved donor (Uthas et al. 2011).

#### 4.4. Magnetic Spotted White Dwarfs

Spotted white dwarfs are difficult to distinguish from reflection-effect binaries like those discussed in Section 4.1. When spectroscopy is not available, we classify all objects with apparently mono-periodic variability and photometrically determined (Gentile Fusillo et al. 2021) masses  $>0.525 M_{\odot}$  and temperatures  $<31,000$  K as isolated white dwarfs with rotational modulation from magnetic spots.

The period of the spot-induced modulations corresponds to the rotational period at the star's surface (e.g., Brinkworth et al. 2013; Kilic et al. 2015; Hoard et al. 2018). We recover the periods of eight previously known spotted white dwarfs from the Gaia DR3 light curves independently, and identify 17 new likely spotted white dwarfs. The majority of the newly identified spotted white dwarfs (12/17) have effective temperatures between 6500 – 10,000 K, placing them inside the range of known DAHe strongly magnetic white dwarfs with Balmer-line emission (Greenstein & McCarthy 1985; Reding et al. 2020; Gänsicke et al. 2020; Walters et al. 2021; Reding et al. 2023; Manser et al. 2023), motivating future time-resolved spectroscopic follow-up. Our sample contains several known DAHe (see Table 2). WD J083531.17+533230.91 ( $G = 18.2$  mag) is the only other

spectroscopically confirmed strongly magnetic white dwarf in our sample, and appears to have a 2.16-hr period.

Examples of three spotted white dwarfs are shown in Figure 5. The top object WD J052026.35+381240.87 ( $G = 15.4$ ) is a spectroscopically confirmed white dwarf from LAMOST claimed to be a DBA (Kong et al. 2019) but is likely a DAH; Gaia DR3 photometry shows it is likely rotating at  $6.7856 \pm 0.0046$  hr. The second object (WD J195629.23–010232.67,  $G = 13.6$  mag) has been known to be spotted (the white dwarf is highly magnetic with a complex field structure, shown in Maxted et al. 2000). We observe clear sinusoidal variability in the *G* data with a period of  $34.898 \pm 0.074$  hr, in close agreement with the literature value from Brinkworth et al. (2005). The final object is WD J202932.51+070107.70 ( $G = 16.6$  mag), a known DO white dwarf (Dreizler et al. 1995). This white dwarf was observed to have a ZTF *g* photometric variability period of  $6.97882 \pm 0.00012$  hr from Reindl et al. (2021), which is close to our LLS fit to the Gaia-*G* data of  $6.9572 \pm 0.0022$  hr. It is likely that the ZTF or Gaia data has selected an incorrect alias due to gaps in the data.

Figure 6 demonstrates Gaia DR3 light curves are able to recover the variability in two of the shortest-period spotted white dwarfs known. The top panel details WD J031715.85–853225.56 ( $G = 14.8$  mag), a well-studied, rapidly rotating, high-field magnetic white dwarf (Ferrario et al. 1997). The Gaia *G* peak occurs at the same period as the TESS data, to within the uncertainties of the LLS fits. The light curve from Gaia is sparsely sampled, with visits separated by  $32.5 \pm 8.8$  d, where  $8.8$  d is the standard deviation of the time between visits. False-alarm probability lines for periodograms are estimated by holding the time sampling the same but randomly shuffling the fluxes with replacement 10,000 times, in an attempt to quantify the probability that the amplitude of a peak can be generated by pure noise (e.g., Greiss et al. 2014; VanderPlas 2018). For WD J031715.85–853225.56 at the top of Figure 6, none of our bootstrapped periodograms have a peak as high as the observed Gaia *G* periodogram, yielding a false-alarm probability of  $<0.1\%$ .

In the bottom panel of Figure 6 we show Gaia and TESS peaks measured for the strongly magnetic, emission-line (DAHe) white dwarf WD J125230.93–023417.72 ( $G = 17.5$  mag, Reding et al. 2020). While not statistically significant, the highest peak in the Gaia periodogram occurs at the known dominant period of 317.278 s (which is the first harmonic the 634.56-s rotation period, see Farihi et al. 2023). We bootstrap a false-alarm probability of 0.1% for this peak.

Aside from these two previously known spotted white dwarfs, we recover the literature periods for six other known spots. Two are known emission-line DAs: the 36.3-min DAHe system WD J003512.88–122508.84 (Reding et al. 2023) and the 2.29-hr, non-magnetic DAe white

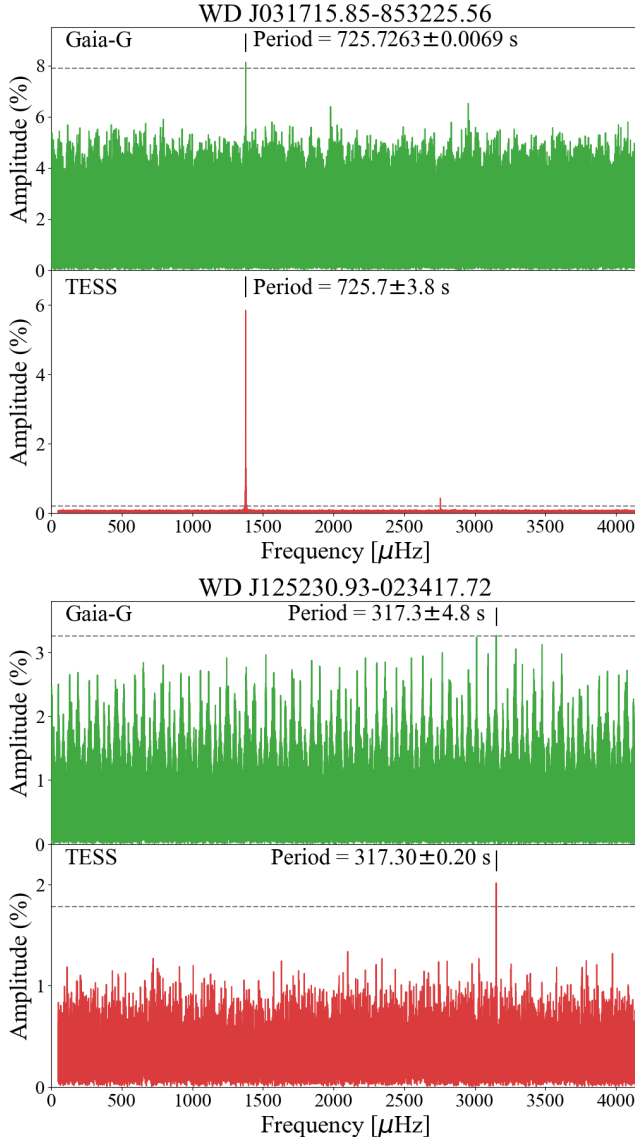


**Figure 6.** Lomb-Scargle periodograms showing two rapidly rotating spotted white dwarfs recovered in sparsely sampled Gaia DR3 light curves. At top is WD J031715.85–853225.56 (Ferrario et al. 1997); the 725 s variability period has a <0.1% false-alarm probability in the Gaia  $G$  light curve. At bottom is WD J125230.93–023417.72, which has a 0.1% false-alarm probability, with the highest peak in the periodogram at exactly the same period, within the uncertainties, as the known variability discovered by Reding et al. (2020).

dwarf WD J041246.84+754942.26 (Tremblay et al. 2020; Elms et al. 2023). We recover two cooler white dwarfs with spots: the 0.72-hr WD J053432.93+770757.40 (Guidry et al. 2021) and the 1.44-d WD J195629.23–010232.67 shown in Figure 5. We also recover two much hotter spotted stars discussed at the end of Section 3, the 6.98-hr WD J202932.51+070107.70 (Reindl et al. 2021) and the 3.45-d WD J095125.94+530930.72 (Werner et al. 2019).

The shortest-period new spotted white dwarf in our sample is WD J115033.35–063618.07 ( $G = 16.4$  mag). This spotted white dwarf features a highest peak in the  $G$  light curve matching the TESS-significant peak at  $884.0679 \pm 0.0094$  s. Spectropolarimetry puts a  $3\sigma$  upper limit on the magnetic field of LP 673-41 of <6 kG (Kawka & Vennes 2012), raising questions about the origin of the spot on this 8600 K white dwarf. The longest period spot appears on WD J124740.10+303007.41 ( $G = 17.9$  mag), with a highest peak in the periodogram at 9.487 d in both its Gaia and ZTF light curves.

#### 4.5. Pulsating White Dwarfs

Pulsating white dwarfs are variable due to non-radial pulsations, with periods typically ranging from 100 – 1500 s, amplitudes up to several percent, and usually multiple, non-harmonically related periods present at the same time (Fontaine & Brassard 2008; Winget & Kepler 2008b). DA white dwarfs are unstable to pulsations in a narrow temperature range between roughly 13,500 – 10,500 K (Hermes et al. 2017c). These hydrogen-atmosphere pulsators are commonly known as ZZ Ceti and DAVs.

From Gaia DR3 photometry alone we are able to independently identify the periods for two new candidate pulsating white dwarfs and confirm the periods of two known DAVs. All objects lie within the empirical DAV instability strip in the Gaia color-magnitude diagram (Figure 1), and their Lomb-Scargle periodograms are shown in Figure 7. As with our spotted white dwarfs in Figure 5, we bootstrap false-alarm probabilities to assess the significance of a peak in the periodogram and quantify the likelihood a peak cannot arise from noise alone. The significance lines in Figure 7 are the 99.9% confidence line (<0.1% false alarm); false-alarm probabilities for all objects in this manuscript are listed in Table 3. While none of our pulsating white dwarfs have formally significant peaks, the chance that the highest peak in the periodogram exactly matches significant peaks in an independent ZTF or TESS dataset is exceptionally low; our periodograms all have step sizes of  $0.01 \mu\text{Hz}$  and run beyond 4000  $\mu\text{Hz}$ , giving hundreds of thousands of trial frequencies. In three of the four cases in Figure 7, the false-alarm probability is <10%.

We find WD J120650.89 –380549.23 ( $G = 15.7$  mag) is a new pulsating WD with a pulsation period at  $259.9127 \pm 0.0013$  s in  $G$  with a 8.1% false-alarm probability that is also significantly detected in TESS. WD J215823.88–585353.81 ( $G = 15.8$  mag) is a known DAV with multiple detected modes from rotational splittings revealed by TESS at 310.27 s, 309.79 s, and 309.31 s (Romero et al. 2022). The highest peak in the  $G_{RP}$  periodogram is consistent with this pulsational variability, at a period of  $310.0049 \pm 0.0021$  s, though this peak has a marginal 28.9% false-alarm

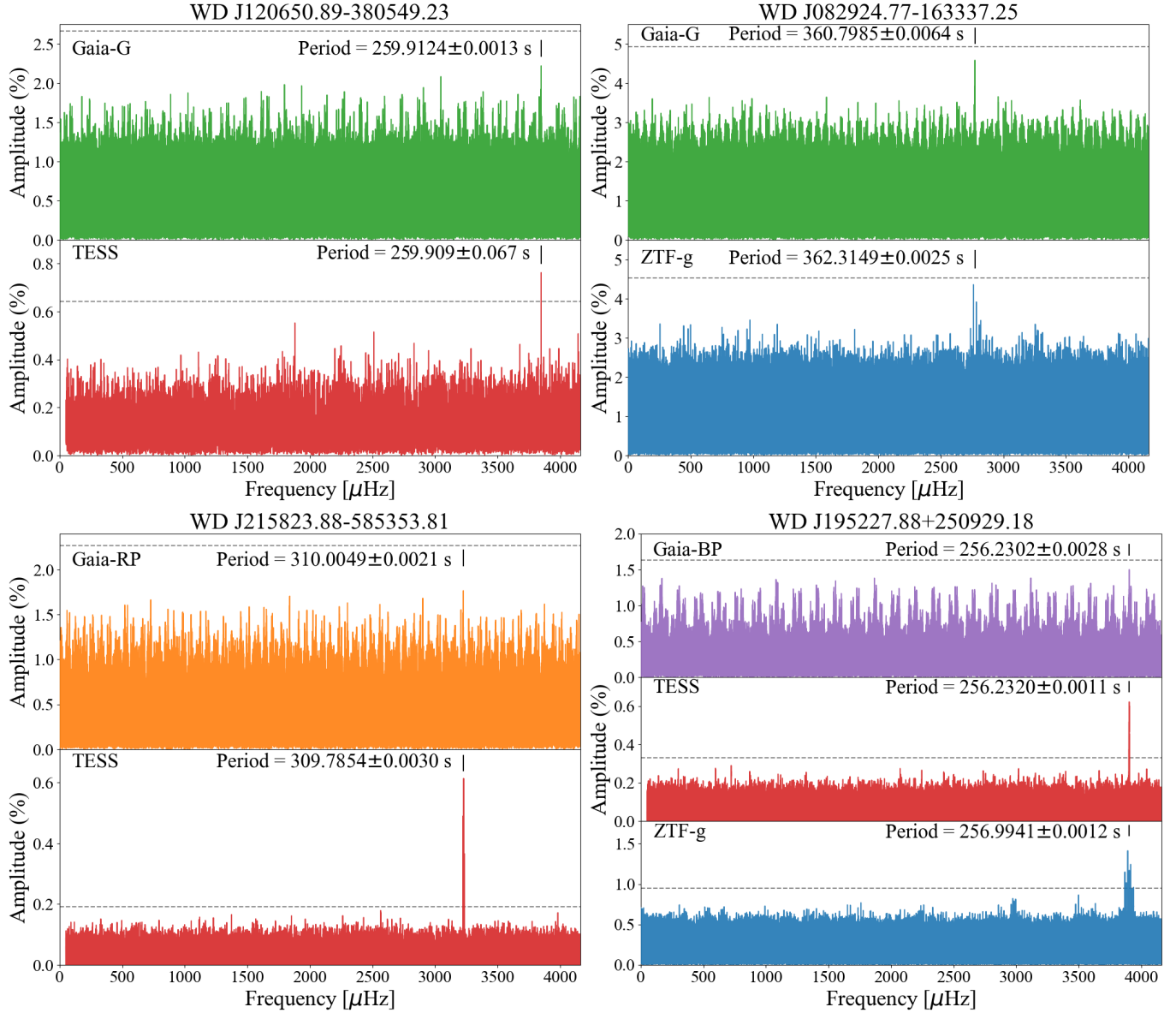


**Figure 7.** Panels of periodograms for the four objects we classify as Gaia-detected pulsating white dwarfs, all with periods  $<400$  s. The photometric bands in these figures are  $G$ ,  $G_{\text{BP}}$ ,  $G_{\text{RP}}$ ,  $g$ ,  $r$ ,  $T$  (Gaia G, BP, and RP bands, ZTF g and r bands, and the TESS photometry band, respectively). A bootstrapped 99.9% confidence lines is shown as a horizontal dashed line in gray (see description in Section 4.4). The false-alarm probabilities of all four Gaia peaks are all between 2.5% and 28.9% (see Table 3).

probability. WD J082924.77–163337.25 ( $G = 17.6$  mag) was identified as a variable white dwarf in Guidry et al. (2021). We detect variability consistent with pulsations in both the Gaia- $G$  and ZTF- $g$  light curves at  $359.0045 \pm 0.0025$  s, with just a 2.5% false-alarm probability. Finally, WD J195227.88+250929.18 ( $G = 15.1$  mag), is a known DAV with a dominant pulsation period of 256.2 s (Kepler 1984; Fontaine et al. 1980). Our analysis agrees closely with a peak in  $G_{\text{BP}}$  at  $255.999 \pm 0.001$  s and a 3.7% false-alarm probability of matching peaks in ZTF and TESS.

The four white dwarfs with likely pulsations detected in their Gaia light curves all have periods  $<400$  s; longer-period modes are likely unstable over long baselines (Hermes et al. 2017c), suggesting longer-period modes will be hard to detect from Gaia data independently. However, pulsating white dwarfs appear to be the most numerous white dwarfs flagged as variable in Gaia DR3. There is an overdensity of points in Figure 1 near the DAV instability strip relative to the 200-pc sample of white dwarfs in the background. In fact, of the 883 candidate white dwarfs that are flagged as photometrically variable in Gaia DR3 with  $P_{\text{WD}} > 0.98$  and

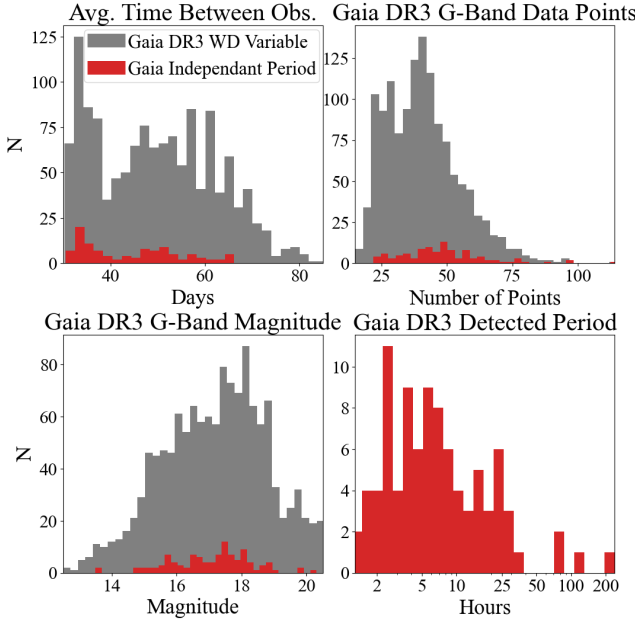


**Figure 8.** Top left histogram shows the average time between Gaia DR3 observations (ignoring the 1 hr 46 min revisit) for the full sample of 1333 candidate white dwarfs flagged as variable in gray, inset in red by the 105 candidate white dwarfs in this manuscript where their variability period can be determined by Gaia independently. The top right panel shows the number of points in each  $G$  light curve, and the bottom left panel shows the  $G$  magnitude distribution of both samples. The bottom right panel shows the distribution of the 105 periods for objects detected by Gaia independently (note that the x-axis is log scale). Although we are slightly more sensitive to objects with more frequent visits, our sample of 105 sources covers most of this parameter space.

masses  $>0.45 M_{\odot}$  from Gentile Fusillo et al. (2021), nearly half (422) have effective temperatures near the DAV instability strip boundaries ( $13,500 > T_{\text{eff}} > 10,500$  K). Literature searches of this sample reveal at least 50 are already-known DAVs, and at least 120 that can be photometrically confirmed with TESS, ZTF or ASAS-SN data; this analysis will be presented in a future publication.

## 5. GAIA-DETECTED PERIODS

We use Gaia DR3 epoch photometry, which includes photometric time series data in the  $G$ -,  $G_{\text{BP}}$ -, and  $G_{\text{RP}}$ - bands (Eyer et al. 2023). Each time-series data point is a so-called field-of-view transit, after an object has passed through nine consecutive CCD observations, each separated by 4.85 s (Roelens et al. 2018). As the Gaia spacecraft spins, objects will then be re-observed at a cadence separated by 1 hr 46 min (Roelens et al. 2017). The time sampling after this revisit is considerably longer, and different for each source, set by the Gaia scanning law (e.g., Boubert et al. 2021).

We analyze the revisit cadence of these observations by creating a histogram of the average time between each obser-

vation, shown in Figure 8. We ignore the revisit timescale of 1 hr 46 min (set by the 6-hr spin period of Gaia, as discussed in de Bruijne 2012) by excluding time between observations of less than 0.3 days, and find an average time of  $49.7 \pm 12.5$  d between observations for the full sample of 1333 objects (the uncertainty is set by the standard deviation of these revisit times). Of the 105 objects where we can measure variability from the Gaia light curves independently, the average revisit time is  $44.2 \pm 10.3$  d. Our subset of 105 objects has slightly less time between observations, only a few more Gaia-G data points (with an average number of points of  $49 \pm 17$  compared to  $41 \pm 14$  for the full sample), and is slightly brighter (with an average magnitude of  $G = 17.0 \pm 1.2$  mag compared to  $G = 17.2 \pm 1.6$  mag for the full sample). The distributions in Figure 8 show we are not heavily biased towards objects with frequent revisits set by the Gaia scanning law. The average and standard deviation in the revisit times between FoV transits for each object is included in Table 3. Among the 72 of 105 objects with ZTF data, the average object has 393 ZTF visits, which is completely consistent with the typical sky coverage of the average fields in ZTF DR12.

We also analyze short-period variability in the Gaia DR3 light curves, which is measured as the object moves from one CCD to the next every 4.85 s (e.g., Roelens et al. 2018). Included in DR3 are per-CCD least-squares fits listed as “Frequency” for objects flagged as vari\_short\_timescale, for select objects with candidate variability periods shorter than 0.5 d. The inverse of the vari\_short\_timescale frequency is listed in Table 2 as  $P_{\text{G,S}}$ , and we check each period generated by our LLS fit ( $P_{\text{G,DR3}}$  in Table 3) against  $P_{\text{G,S}}$ . In our final 105 object sample, 65 objects are flagged in Gaia DR3 as short-timescale sources, and 55 of these 65 (85%) have  $P_{\text{G,S}}$  that matches  $P_{\text{G,DR3}}$  to within 3% (after which the agreement is never better than 22%).

We compare the Gaia DR3 short-timescale analysis against our LLS fits by object type. We find that of our 72 binary objects, 48 of 53 (91%) with vari\_short\_timescale data have  $P_{\text{G,S}}$  that matches our determinations of  $P_{\text{G,DR3}}$ , and of the spotted white dwarfs, 5 of 7 with short-timescale analysis match. For all variable types, the Gaia DR3 short-timescale analysis returns 55/60 (92%) matches for objects with vari\_short\_timescale between 0.278 and 2.78 hours, and routinely does poorly for periods longer than 3 hr.

We also attempt to assess the reliability of the Gaia variability identifier (Eyer et al. 2023). Gaia uses a machine learning algorithm trained on non-variable objects and then tested against training sets (built from various published catalogues of variable stars) to confirm how effectively this algorithm can identify variable objects. Objects are categorized as variable when there is a large value for the ratio of the difference in magnitude from the average for that object to the interquartile range of the magnitude. These objects are then

passed through one of two paths in the machine learning process to be sorted into a specific Gaia “class,” discussed in depth in Rimoldini et al. (2023). This Gaia class is listed in Table 2.

We find that this “class” is not generally useful, as most are simply “WD.” There is one case where this class correctly identifies a known CV (WDJ130017.86–325805.23). The Gaia “class” also marks two objects as “S” or stars with short-timescale variability: WD J083843.35–282701.14 (a known CV with  $P_{G,S}$  that matches  $P_{G,DR3}$  at  $16.109 \pm 0.029$  hr) and WD J233923.79–485350.19 (a likely new binary system with  $P_{G,S}$  that matches  $P_{G,DR3}$  at  $2.52962 \pm 0.00075$  hr). The new eclipsing CV WD J154008.28–392917.61 also has a Gaia “class” of CV.

Finally, we note that Gaia epoch photometry may contain spurious periodicities due to scan-angle-dependent signals, especially in marginally resolved, fixed-orientation pairs of stars separated by  $<0.5$  arcsec (Holl et al. 2023). Although previous work has only explored signals up to 10 days, and most signals determined here are below that, we investigate the likelihood that any of our detections are spurious.

All 1333 white dwarf candidates in our sample have information in the `vari_spurious_signals` table from Holl et al. (2023), including important metrics that can reveal close binarity, the Spearman rank correlation coefficient with corrected flux excess factor ( $r_{\text{exf},G}$ ) and the Image Parameter Determination model ( $r_{\text{ipd},G}$ ). Only three white dwarfs have both  $r_{\text{exf},G}$  and  $r_{\text{ipd},G}$  values  $>0.8$  (WD J020426.03+571026.62, WD J031047.57–100153.85, and WD J100643.74–221757.86), none of which are included in our subset of 105 white dwarfs with variability measured independently from Gaia. In our subset of 105 objects, only one has  $r_{\text{ipd},G} > 0.6$  and that is WD J003512.88–122508.84, which has confirmed variability from TESS (Reding et al. 2023). We conclude that contamination from spurious Gaia scanning-law-dependent periods is unlikely in our sample of white dwarfs.

## 6. DISCUSSION & CONCLUSIONS

We analyze 105 white dwarf candidates for which Gaia is capable of detecting accurate periods from DR3 photometry. These periods of variability range from 9.5 d to as short as 256.2 s (roughly 4 min), including seven objects with periods shorter than 1000 s. We obtained this result by comparing Gaia multi-band photometry to data from ZTF and TESS to identify significant periods within the Gaia data. Analysis of the Gaia photometry resulted in the discovery of new pulsating, spotted and binary white dwarfs. This includes a new 68.4-min eclipsing cataclysmic variable, which has a period well below the CV period minimum of roughly 80 min (Knigge et al. 2011) and is one of the shortest-period CVs known.

Our overall analysis demonstrates that Gaia epoch photometry is precise enough to detect short-term, low-amplitude periods even when observations are sparsely sampled. The absolute median amplitude of the photometric variability we confirm from Gaia independently is 1.4%, with an average period of roughly 12 hr. This is notable compared to the distribution of time between observations, which is on average roughly 44 d. We find that overall, the 105 variables that are significant in Gaia are slightly brighter and sampled more often than the full sample of 1333 objects, but the distributions of magnitudes or number of points are not significantly biased in either parameter space, as shown in Figure 8.

The likelihood that the highest peak in two independent periodograms match is small, given that there are more than  $10^5$  frequency elements in each periodogram. This is the basis for which we claim Gaia has detected a periodicity. Still, we have bootstrapped estimates that a peak in the periodogram can be caused by noise alone and find that 33/105 objects have significant peaks in their Gaia light curves, with a  $<0.1\%$  false-alarm probability. Nearly half the sample, 50/105, have peaks with a false alarm  $<1\%$ . Only three have  $>35\%$ , but all 105 have Gaia peaks with a  $<41\%$  false-alarm probability (Table 3 details this value for all objects in our sample). Our work provides an empirically determined set of cutoffs for which variability in a Gaia DR3 light curve is likely to be genuine, and it also represents a useful value for future analysis of sparsely sampled, high-precision photometry from large surveys like the Vera C. Rubin Observatory and its Legacy Survey of Space and Time (LSST; Ivezić et al. 2019), as well as the Nancy Grace Roman Space Telescope (Akeson et al. 2019).

Previous spectroscopy exists for only 36 of the 105 objects discussed in this paper, so follow up is encouraged for most of these sources. There are many objects of interest that would expand sample sizes of rare object types. Some notable examples include WD J123955.40+834707.51 ( $G = 20.0$  mag), which may be a new WD+WD binary containing an ELM white dwarf, and WD J130017.86–325805.23 ( $G = 20.3$  mag) which is a candidate CV with recorded outbursts (Drake et al. 2014) but shows a dominant photometric period of 36.2 min closer to the orbital period of AM CVn binaries (see Section 4.1). There are also multiple candidate eclipsing binaries discussed in Section 4.3. Finally, one of the shortest-period new spotted white dwarfs we discovered here (WD J115033.35–063618.07) appears to have an 884.73-s spin period but a  $<6$  kG magnetic field, raising questions about the origin of its fast rotation (see Section 4.4).

As Gaia continues to scan the sky, the methods discussed in this paper provide a foundation for analyzing short-period variables within even longer-baseline data. Verifying that Gaia data independently can be used to detect short periods will allow future work on sources with no additional spectro-

scopic or photometric information. Increasing the numbers of rare variable stellar remnants, especially those in short-period binaries or with magnetic spots, will help constrain their space density and formation channels.

## 7. ACKNOWLEDGEMENTS

The authors thank the anonymous referee for a very useful report, as well as fruitful discussions with Stu Littlefair. Support for this work was in part provided by NASA TESS Cycle 2 Grant 80NSSC20K0592 and Cycle 4 grant 80NSSC22K0737, as well as the National Science Foundation under grant No. NSF PHY-1748958, as portions of this project were completed at the KITP Program “White Dwarfs as Probes of the Evolution of Planets, Stars, the Milky Way and the Expanding Universe.”

The authors acknowledge the European Southern Observatory program 110.23UU.001, as well as the Transiting Exoplanet Survey Satellite (TESS), the Zwicky Transiting Facility (ZTF), the All-Sky Automated Survey for Supernovae (ASAS-SN), and the Asteroid Terrestrial-impact Last Alert System (ATLAS) for the public release of all-sky photometry data for many of these objects. This work has also made use of data from the European Space Agency

(ESA) mission *Gaia* (<https://www.cosmos.esa.int/gaia>), processed by the *Gaia* Data Processing and Analysis Consortium (DPAC, <https://www.cosmos.esa.int/web/gaia/dpac/consortium>). Funding for the DPAC has been provided by national institutions, in particular the institutions participating in the *Gaia* Multilateral Agreement.

This research is also based on observations obtained at the Southern Astrophysical Research (SOAR) telescope, which is a joint project of the Ministério da Ciência, Tecnologia e Inovações (MCTI/LNA) do Brasil, the US National Science Foundation’s NOIRLab, the University of North Carolina at Chapel Hill (UNC), and Michigan State University (MSU).

**Facilities:** The Gaia Collaboration, The Zwicky Transient Facility, The Transiting Exoplanet Survey Satellite, NTT, SOAR

**Software:** astropy (Astropy Collaboration et al. 2013, 2018), numpy (Harris et al. 2020), lightkurve (Lightkurve Collaboration et al. 2018), pandas (Reback et al. 2022), astroquery (Ginsburg et al. 2019), matplotlib (Hunter 2007), lmfit (Newville et al. 2016), TOPCAT (Taylor 2005)

## REFERENCES

- Akeson, R., Armus, L., Bachelet, E., et al. 2019, arXiv e-prints, arXiv:1902.05569, doi: [10.48550/arXiv.1902.05569](https://doi.org/10.48550/arXiv.1902.05569)
- Astropy Collaboration, Robitaille, T. P., Tollerud, E. J., et al. 2013, A&A, 558, A33, doi: [10.1051/0004-6361/201322068](https://doi.org/10.1051/0004-6361/201322068)
- Astropy Collaboration, Price-Whelan, A. M., Sipőcz, B. M., et al. 2018, AJ, 156, 123, doi: [10.3847/1538-3881/aabc4f](https://doi.org/10.3847/1538-3881/aabc4f)
- Astropy Collaboration, Price-Whelan, A. M., Lim, P. L., et al. 2022, ApJ, 935, 167, doi: [10.3847/1538-4357/ac7c74](https://doi.org/10.3847/1538-4357/ac7c74)
- Badenes, C., van Kerwijk, M. H., Kilic, M., et al. 2013, MNRAS, 429, 3596, doi: [10.1093/mnras/sts646](https://doi.org/10.1093/mnras/sts646)
- Bellm, E. C., Kulkarni, S. R., Graham, M. J., et al. 2019, PASP, 131, 018002, doi: [10.1088/1538-3873/aaecbe](https://doi.org/10.1088/1538-3873/aaecbe)
- Bond, H. E., Chanmugam, G., & Grauer, A. 1979, ApJL, 234, L113, doi: [10.1086/183120](https://doi.org/10.1086/183120)
- Boubert, D., Everall, A., Fraser, J., Gration, A., & Holl, B. 2021, MNRAS, 501, 2954, doi: [10.1093/mnras/staa3791](https://doi.org/10.1093/mnras/staa3791)
- Bours, M. C. P., Marsh, T. R., Parsons, S. G., et al. 2016, MNRAS, 460, 3873, doi: [10.1093/mnras/stw1203](https://doi.org/10.1093/mnras/stw1203)
- Breger, M., Stich, J., Garrido, R., et al. 1993, A&A, 271, 482
- Brinkworth, C. S., Burleigh, M. R., Lawrie, K., Marsh, T. R., & Knigge, C. 2013, ApJ, 773, 47, doi: [10.1088/0004-637X/773/1/47](https://doi.org/10.1088/0004-637X/773/1/47)
- Brinkworth, C. S., Marsh, T. R., Morales-Rueda, L., et al. 2005, MNRAS, 357, 333, doi: [10.1111/j.1365-2966.2005.08649.x](https://doi.org/10.1111/j.1365-2966.2005.08649.x)
- Brown, W. R., Kilic, M., Kosakowski, A., & Gianninas, A. 2022, ApJ, 933, 94, doi: [10.3847/1538-4357/ac72ac](https://doi.org/10.3847/1538-4357/ac72ac)
- Burdge, K. B., Prince, T. A., Fuller, J., et al. 2020, ApJ, 905, 32, doi: [10.3847/1538-4357/abc261](https://doi.org/10.3847/1538-4357/abc261)
- Calamida, A., Matheson, T., Olszewski, E. W., et al. 2022, ApJ, 940, 19, doi: [10.3847/1538-4357/ac96f4](https://doi.org/10.3847/1538-4357/ac96f4)
- Chidester, M. T., Farag, E., & Timmes, F. X. 2022, ApJ, 935, 21, doi: [10.3847/1538-4357/ac7ec3](https://doi.org/10.3847/1538-4357/ac7ec3)
- Clemens, J. C., Crain, J. A., & Anderson, R. 2004, in Society of Photo-Optical Instrumentation Engineers (SPIE) Conference Series, Vol. 5492, Ground-based Instrumentation for Astronomy, ed. A. F. M. Moorwood & M. Iye, 331–340, doi: [10.1117/12.550069](https://doi.org/10.1117/12.550069)
- Cánovas, H., & de Bruijne, J. 2022, Datalink Python Access, European Space Agency. <https://www.cosmos.esa.int/web/gaia-users/archive/datalink-products>
- de Bruijne, J. H. J. 2012, Ap&SS, 341, 31, doi: [10.1007/s10509-012-1019-4](https://doi.org/10.1007/s10509-012-1019-4)
- Dhillon, V. S., Marsh, T. R., Stevenson, M. J., et al. 2007, MNRAS, 378, 825, doi: [10.1111/j.1365-2966.2007.11881.x](https://doi.org/10.1111/j.1365-2966.2007.11881.x)
- Dhillon, V. S., Bezawada, N., Black, M., et al. 2021, MNRAS, 507, 350, doi: [10.1093/mnras/stab2130](https://doi.org/10.1093/mnras/stab2130)
- Drake, A. J., Beshore, E., Catelan, M., et al. 2010, arXiv e-prints, arXiv:1009.3048. <https://arxiv.org/abs/1009.3048>

- Drake, A. J., Gänsicke, B. T., Djorgovski, S. G., et al. 2014, Monthly Notices of the Royal Astronomical Society, 441, 1186, doi: [10.1093/mnras/stu639](https://doi.org/10.1093/mnras/stu639)
- Drake, A. J., Graham, M. J., Djorgovski, S. G., et al. 2014, ApJS, 213, 9, doi: [10.1088/0067-0049/213/1/9](https://doi.org/10.1088/0067-0049/213/1/9)
- Drake, A. J., Djorgovski, S. G., Catelan, M., et al. 2017, MNRAS, 469, 3688, doi: [10.1093/mnras/stx1085](https://doi.org/10.1093/mnras/stx1085)
- Dreizler, S., Heber, U., Napiwotzki, R., & Hagen, H. J. 1995, A&A, 303, L53
- Dufour, P., Blouin, S., Coutu, S., et al. 2017, in Astronomical Society of the Pacific Conference Series, Vol. 509, 20th European White Dwarf Workshop, ed. P. E. Tremblay, B. Gaensicke, & T. Marsh, 3. <https://arxiv.org/abs/1610.00986>
- Eisenstein, D. J., Liebert, J., Harris, H. C., et al. 2006, ApJS, 167, 40, doi: [10.1086/507110](https://doi.org/10.1086/507110)
- Elms, A. K., Tremblay, P.-E., Gänsicke, B. T., et al. 2023, MNRAS, 524, 4996, doi: [10.1093/mnras/stad2171](https://doi.org/10.1093/mnras/stad2171)
- Eyer, L., Audard, M., Holl, B., et al. 2023, A&A, 674, A13, doi: [10.1051/0004-6361/202244242](https://doi.org/10.1051/0004-6361/202244242)
- Farihi, J., Hermes, J. J., Littlefair, S. P., et al. 2023, MNRAS, 525, 1097, doi: [10.1093/mnras/stad2184](https://doi.org/10.1093/mnras/stad2184)
- Ferrario, L., Vennes, S., Wickramasinghe, D. T., Bailey, J. A., & Christian, D. J. 1997, MNRAS, 292, 205, doi: [10.1093/mnras/292.2.205](https://doi.org/10.1093/mnras/292.2.205)
- Fontaine, G., & Brassard, P. 2008, PASP, 120, 1043, doi: [10.1086/592788](https://doi.org/10.1086/592788)
- Fontaine, G., McGraw, J. T., Coleman, L., et al. 1980, ApJ, 239, 898, doi: [10.1086/158176](https://doi.org/10.1086/158176)
- Fuller, J., Piro, A. L., & Jermyn, A. S. 2019, MNRAS, 485, 3661, doi: [10.1093/mnras/stz514](https://doi.org/10.1093/mnras/stz514)
- Gaia Collaboration, Eyer, L., Rimoldini, L., et al. 2019, A&A, 623, A110, doi: [10.1051/0004-6361/201833304](https://doi.org/10.1051/0004-6361/201833304)
- Gaia Collaboration, De Ridder, J., Ripepi, V., et al. 2023a, A&A, 674, A36, doi: [10.1051/0004-6361/202243767](https://doi.org/10.1051/0004-6361/202243767)
- Gaia Collaboration, Vallenari, A., Brown, A. G. A., et al. 2023b, A&A, 674, A1, doi: [10.1051/0004-6361/202243940](https://doi.org/10.1051/0004-6361/202243940)
- . 2023c, A&A, 674, A1, doi: [10.1051/0004-6361/202243940](https://doi.org/10.1051/0004-6361/202243940)
- Gänsicke, B. T., Rodríguez-Gil, P., Gentile Fusillo, N. P., et al. 2020, MNRAS, 499, 2564, doi: [10.1093/mnras/staa2969](https://doi.org/10.1093/mnras/staa2969)
- Gavras, P., Rimoldini, L., Nienartowicz, K., et al. 2023, A&A, 674, A22, doi: [10.1051/0004-6361/202244367](https://doi.org/10.1051/0004-6361/202244367)
- Gentile Fusillo, N. P., Tremblay, P. E., Cukanovaite, E., et al. 2021, MNRAS, 508, 3877, doi: [10.1093/mnras/stab2672](https://doi.org/10.1093/mnras/stab2672)
- Giannicchele, N., Charpinet, S., Fontaine, G., et al. 2018, Nature, 554, 73, doi: [10.1038/nature25136](https://doi.org/10.1038/nature25136)
- Ginsburg, A., Sipőcz, B. M., Brasseur, C. E., et al. 2019, AJ, 157, 98, doi: [10.3847/1538-3881/aafc33](https://doi.org/10.3847/1538-3881/aafc33)
- Greenstein, J. L., & McCarthy, J. K. 1985, ApJ, 289, 732, doi: [10.1086/162937](https://doi.org/10.1086/162937)
- Greiss, S., Gänsicke, B. T., Hermes, J. J., et al. 2014, MNRAS, 438, 3086, doi: [10.1093/mnras/stt2420](https://doi.org/10.1093/mnras/stt2420)
- Gidry, J. A., Vanderbosch, Z. P., Hermes, J. J., et al. 2021, ApJ, 912, 125, doi: [10.3847/1538-4357/abee68](https://doi.org/10.3847/1538-4357/abee68)
- Hallakoun, N., Maoz, D., Kilic, M., et al. 2016, MNRAS, 458, 845, doi: [10.1093/mnras/stw364](https://doi.org/10.1093/mnras/stw364)
- Hallakoun, N., Maoz, D., Agol, E., et al. 2018, MNRAS, 476, 933, doi: [10.1093/mnras/sty257](https://doi.org/10.1093/mnras/sty257)
- Halpern, J. P., Bogdanov, S., & Thorstensen, J. R. 2017, ApJ, 838, 124, doi: [10.3847/1538-4357/838/2/124](https://doi.org/10.3847/1538-4357/838/2/124)
- Harris, C. R., Millman, K. J., van der Walt, S. J., et al. 2020, Nature, 585, 357, doi: [10.1038/s41586-020-2649-2](https://doi.org/10.1038/s41586-020-2649-2)
- Heintz, T. M., Hermes, J. J., El-Badry, K., et al. 2022, ApJ, 934, 148, doi: [10.3847/1538-4357/ac78d9](https://doi.org/10.3847/1538-4357/ac78d9)
- Hermes, J. J., Gänsicke, B. T., Gentile Fusillo, N. P., et al. 2017a, MNRAS, 468, 1946, doi: [10.1093/mnras/stx567](https://doi.org/10.1093/mnras/stx567)
- Hermes, J. J., Kawaler, S. D., Bischoff-Kim, A., et al. 2017b, ApJ, 835, 277, doi: [10.3847/1538-4357/835/2/277](https://doi.org/10.3847/1538-4357/835/2/277)
- Hermes, J. J., Gänsicke, B. T., Bischoff-Kim, A., et al. 2015, MNRAS, 451, 1701, doi: [10.1093/mnras/stv1053](https://doi.org/10.1093/mnras/stv1053)
- Hermes, J. J., Gänsicke, B. T., Kawaler, S. D., et al. 2017c, ApJS, 232, 23, doi: [10.3847/1538-4365/aa8bb5](https://doi.org/10.3847/1538-4365/aa8bb5)
- Hoard, D. W., Howell, S. B., Roettenbacher, R. M., et al. 2018, AJ, 156, 119, doi: [10.3847/1538-3881/aad238](https://doi.org/10.3847/1538-3881/aad238)
- Holberg, J. B., & Howell, S. B. 2011, AJ, 142, 62, doi: [10.1088/0004-6256/142/2/62](https://doi.org/10.1088/0004-6256/142/2/62)
- Holl, B., Fabricius, C., Portell, J., et al. 2023, A&A, 674, A25, doi: [10.1051/0004-6361/202245353](https://doi.org/10.1051/0004-6361/202245353)
- Hollands, M. A., Tremblay, P. E., Gänsicke, B. T., Gentile-Fusillo, N. P., & Toonen, S. 2018, MNRAS, 480, 3942, doi: [10.1093/mnras/sty2057](https://doi.org/10.1093/mnras/sty2057)
- Howell, S. B., Everett, M. E., Seebode, S. A., et al. 2013, AJ, 145, 109, doi: [10.1088/0004-6256/145/4/109](https://doi.org/10.1088/0004-6256/145/4/109)
- Hunter, J. D. 2007, Computing in Science and Engineering, 9, 90, doi: [10.1109/MCSE.2007.55](https://doi.org/10.1109/MCSE.2007.55)
- Ivezić, Ž., Kahn, S. M., Tyson, J. A., et al. 2019, ApJ, 873, 111, doi: [10.3847/1538-4357/ab042c](https://doi.org/10.3847/1538-4357/ab042c)
- Kalomeni, B., Nelson, L., Rappaport, S., et al. 2016, ApJ, 833, 83, doi: [10.3847/1538-4357/833/1/83](https://doi.org/10.3847/1538-4357/833/1/83)
- Kao, W., Kaplan, D. L., Prince, T. A., et al. 2016, MNRAS, 461, 2747, doi: [10.1093/mnras/stw1434](https://doi.org/10.1093/mnras/stw1434)
- Kawka, A., & Vennes, S. 2012, MNRAS, 425, 1394, doi: [10.1111/j.1365-2966.2012.21574.x](https://doi.org/10.1111/j.1365-2966.2012.21574.x)
- Kepler, S. O. 1984, ApJ, 278, 754, doi: [10.1086/161845](https://doi.org/10.1086/161845)
- Kepler, S. O., Pelisoli, I., Koester, D., et al. 2015, MNRAS, 446, 4078, doi: [10.1093/mnras/stu2388](https://doi.org/10.1093/mnras/stu2388)
- . 2016, MNRAS, 455, 3413, doi: [10.1093/mnras/stv2526](https://doi.org/10.1093/mnras/stv2526)
- Kilic, M., Gianninas, A., Bell, K. J., et al. 2015, ApJL, 814, L31, doi: [10.1088/2041-8205/814/2/L31](https://doi.org/10.1088/2041-8205/814/2/L31)

- Kilkenny, D., O'Donoghue, D., Worters, H. L., et al. 2015, MNRAS, 453, 1879, doi: [10.1093/mnras/stv1771](https://doi.org/10.1093/mnras/stv1771)
- Kilkenny, D., Worters, H. L., O'Donoghue, D., et al. 2016, MNRAS, 459, 4343, doi: [10.1093/mnras/stw916](https://doi.org/10.1093/mnras/stw916)
- Kleinman, S. J., Kepler, S. O., Koester, D., et al. 2013, ApJS, 204, 5, doi: [10.1088/0067-0049/204/1/5](https://doi.org/10.1088/0067-0049/204/1/5)
- Knigge, C., Baraffe, I., & Patterson, J. 2011, ApJS, 194, 28, doi: [10.1088/0067-0049/194/2/28](https://doi.org/10.1088/0067-0049/194/2/28)
- Kochanek, C. S., Shappee, B. J., Stanek, K. Z., et al. 2017, PASP, 129, 104502, doi: [10.1088/1538-3873/aa80d9](https://doi.org/10.1088/1538-3873/aa80d9)
- Koester, D., Napiwotzki, R., Christlieb, N., et al. 2001, A&A, 378, 556, doi: [10.1051/0004-6361:20011235](https://doi.org/10.1051/0004-6361:20011235)
- Kong, X., Luo, A. L., & Li, X.-R. 2019, Research in Astronomy and Astrophysics, 19, 088, doi: [10.1088/1674-4527/19/6/88](https://doi.org/10.1088/1674-4527/19/6/88)
- Kosakowski, A., Kilic, M., Brown, W. R., Bergeron, P., & Kupfer, T. 2022, MNRAS, 516, 720, doi: [10.1093/mnras/stac1146](https://doi.org/10.1093/mnras/stac1146)
- Kosakowski, A., Kilic, M., Brown, W. R., & Gianninas, A. 2020, ApJ, 894, 53, doi: [10.3847/1538-4357/ab8300](https://doi.org/10.3847/1538-4357/ab8300)
- Liebert, J., Green, R. F., Wesemael, F., & Margon, B. 1981, AJ, 86, 1384, doi: [10.1086/113018](https://doi.org/10.1086/113018)
- Lightkurve Collaboration, Cardoso, J. V. d. M., Hedges, C., et al. 2018, Lightkurve: Kepler and TESS time series analysis in Python, Astrophysics Source Code Library. <http://ascl.net/1812.013>
- Littlefair, S. P., Dhillon, V. S., Marsh, T. R., et al. 2007, MNRAS, 381, 827, doi: [10.1111/j.1365-2966.2007.12285.x](https://doi.org/10.1111/j.1365-2966.2007.12285.x)
- Manser, C. J., Gänsicke, B. T., Ingham, K., et al. 2023, MNRAS, 521, 4976, doi: [10.1093/mnras/stad727](https://doi.org/10.1093/mnras/stad727)
- Maoz, D., Mazeh, T., & McQuillan, A. 2015, MNRAS, 447, 1749, doi: [10.1093/mnras/stu2577](https://doi.org/10.1093/mnras/stu2577)
- Marsh, T. R., & Duck, S. R. 1996, MNRAS, 278, 565, doi: [10.1093/mnras/278.2.565](https://doi.org/10.1093/mnras/278.2.565)
- Marton, G., Ábrahám, P., Rimoldini, L., et al. 2023, A&A, 674, A21, doi: [10.1051/0004-6361/202244101](https://doi.org/10.1051/0004-6361/202244101)
- Maxted, P. F. L., Ferrario, L., Marsh, T. R., & Wickramasinghe, D. T. 2000, MNRAS, 315, L41, doi: [10.1046/j.1365-8711.2000.03636.x](https://doi.org/10.1046/j.1365-8711.2000.03636.x)
- McAllister, M., Littlefair, S. P., Parsons, S. G., et al. 2019, MNRAS, 486, 5535, doi: [10.1093/mnras/stz976](https://doi.org/10.1093/mnras/stz976)
- Mickaelian, A. M. 2008, AJ, 136, 946, doi: [10.1088/0004-6256/136/3/946](https://doi.org/10.1088/0004-6256/136/3/946)
- Nebot Gómez-Morán, A., Gänsicke, B. T., Schreiber, M. R., et al. 2011, A&A, 536, A43, doi: [10.1051/0004-6361/201117514](https://doi.org/10.1051/0004-6361/201117514)
- Newville, M., Stensitzki, T., Allen, D. B., et al. 2016, Lmfit: Non-Linear Least-Square Minimization and Curve-Fitting for Python, Astrophysics Source Code Library, record ascl:1606.014. <http://ascl.net/1606.014>.
- Pala, A. F., Gänsicke, B. T., Breedt, E., et al. 2020, MNRAS, 494, 3799, doi: [10.1093/mnras/staa764](https://doi.org/10.1093/mnras/staa764)
- Parsons, S. G., Gänsicke, B. T., Marsh, T. R., et al. 2013, MNRAS, 429, 256, doi: [10.1093/mnras/sts332](https://doi.org/10.1093/mnras/sts332)
- Parsons, S. G., Agurto-Gangas, C., Gänsicke, B. T., et al. 2015, MNRAS, 449, 2194, doi: [10.1093/mnras/stv382](https://doi.org/10.1093/mnras/stv382)
- Parsons, S. G., Gänsicke, B. T., Marsh, T. R., et al. 2017, MNRAS, 470, 4473, doi: [10.1093/mnras/stx1522](https://doi.org/10.1093/mnras/stx1522)
- . 2018, MNRAS, 481, 1083, doi: [10.1093/mnras/sty2345](https://doi.org/10.1093/mnras/sty2345)
- Patterson, J. 1984, ApJS, 54, 443, doi: [10.1086/190940](https://doi.org/10.1086/190940)
- Prochaska, J., Hennawi, J., Westfall, K., et al. 2020, The Journal of Open Source Software, 5, 2308, doi: [10.21105/joss.02308](https://doi.org/10.21105/joss.02308)
- Raddi, R., Gentile Fusillo, N. P., Pala, A. F., et al. 2017, MNRAS, 472, 4173, doi: [10.1093/mnras/stx2243](https://doi.org/10.1093/mnras/stx2243)
- Rea, N., Coti Zelati, F., Esposito, P., et al. 2017, MNRAS, 471, 2902, doi: [10.1093/mnras/stx1560](https://doi.org/10.1093/mnras/stx1560)
- Reback, J., jbrockmendel, McKinney, W., et al. 2022, pandas-dev/pandas: Pandas 1.4.2, v1.4.2, Zenodo, Zenodo, doi: [10.5281/zenodo.3509134](https://doi.org/10.5281/zenodo.3509134)
- Rebassa-Mansergas, A., Gänsicke, B. T., Rodríguez-Gil, P., Schreiber, M. R., & Koester, D. 2007, MNRAS, 382, 1377, doi: [10.1111/j.1365-2966.2007.12288.x](https://doi.org/10.1111/j.1365-2966.2007.12288.x)
- Rebassa-Mansergas, A., Gänsicke, B. T., Schreiber, M. R., Koester, D., & Rodríguez-Gil, P. 2010, MNRAS, 402, 620, doi: [10.1111/j.1365-2966.2009.15915.x](https://doi.org/10.1111/j.1365-2966.2009.15915.x)
- Reding, J. S., Hermes, J. J., & Clemens, J. C. 2018, in Proceedings of the 21st European Workshop on White Dwarfs, 1, doi: [10.26153/tsw/967](https://doi.org/10.26153/tsw/967)
- Reding, J. S., Hermes, J. J., Clemens, J. C., Hegedus, R. J., & Kaiser, B. C. 2023, MNRAS, 522, 693, doi: [10.1093/mnras/stad760](https://doi.org/10.1093/mnras/stad760)
- Reding, J. S., Hermes, J. J., Vanderbosch, Z., et al. 2020, ApJ, 894, 19, doi: [10.3847/1538-4357/ab8239](https://doi.org/10.3847/1538-4357/ab8239)
- Reindl, N., Schaffenroth, V., Filiz, S., et al. 2021, A&A, 647, A184, doi: [10.1051/0004-6361/202140289](https://doi.org/10.1051/0004-6361/202140289)
- Ren, L., Li, C., Ma, B., et al. 2023, ApJS, 264, 39, doi: [10.3847/1538-4365/aca09e](https://doi.org/10.3847/1538-4365/aca09e)
- Ricker, G. R., Winn, J. N., Vanderspek, R., et al. 2015, Journal of Astronomical Telescopes, Instruments, and Systems, 1, 014003, doi: [10.1117/1.JATIS.1.1.014003](https://doi.org/10.1117/1.JATIS.1.1.014003)
- Rimoldini, L., Holl, B., Gavras, P., et al. 2023, A&A, 674, A14, doi: [10.1051/0004-6361/202245591](https://doi.org/10.1051/0004-6361/202245591)
- Roelens, M., Eyer, L., Mowlavi, N., et al. 2017, MNRAS, 472, 3230, doi: [10.1093/mnras/stx2115](https://doi.org/10.1093/mnras/stx2115)
- . 2018, A&A, 620, A197, doi: [10.1051/0004-6361/201833357](https://doi.org/10.1051/0004-6361/201833357)
- Romero, A. D., Cársico, A. H., Althaus, L. G., et al. 2012, MNRAS, 420, 1462, doi: [10.1111/j.1365-2966.2011.20134.x](https://doi.org/10.1111/j.1365-2966.2011.20134.x)
- Romero, A. D., Kepler, S. O., Hermes, J. J., et al. 2022, MNRAS, 511, 1574, doi: [10.1093/mnras/stac093](https://doi.org/10.1093/mnras/stac093)
- Saunders, N. 2020, Searching & downloading Kepler, K2, and Tess Data, Lightkurve. <https://docs.lightkurve.org/tutorials/1-getting-started/searching-for-data-products.html>

- Savoury, C. D. J., Littlefair, S. P., Dhillon, V. S., et al. 2011, MNRAS, 415, 2025, doi: [10.1111/j.1365-2966.2011.18707.x](https://doi.org/10.1111/j.1365-2966.2011.18707.x)
- Schaffenroth, V., Pelisoli, I., Barlow, B. N., Geier, S., & Kupfer, T. 2022, A&A, 666, A182, doi: [10.1051/0004-6361/202244214](https://doi.org/10.1051/0004-6361/202244214)
- Shappee, B. J., Prieto, J. L., Grupe, D., et al. 2014, ApJ, 788, 48, doi: [10.1088/0004-637X/788/1/48](https://doi.org/10.1088/0004-637X/788/1/48)
- Szkody, P., Dicenzo, B., Ho, A. Y. Q., et al. 2020, AJ, 159, 198, doi: [10.3847/1538-3881/ab7cce](https://doi.org/10.3847/1538-3881/ab7cce)
- Szkody, P., Olde Loohuis, C., Koplitz, B., et al. 2021, AJ, 162, 94, doi: [10.3847/1538-3881/ac0efb](https://doi.org/10.3847/1538-3881/ac0efb)
- Taylor, M. B. 2005, in Astronomical Society of the Pacific Conference Series, Vol. 347, Astronomical Data Analysis Software and Systems XIV, ed. P. Shopbell, M. Britton, & R. Ebert, 29
- Tony, J. L., Denneau, L., Heinze, A. N., et al. 2018, PASP, 130, 064505, doi: [10.1088/1538-3873/aabadf](https://doi.org/10.1088/1538-3873/aabadf)
- Tremblay, P. E., Hollands, M. A., Gentile Fusillo, N. P., et al. 2020, MNRAS, 497, 130, doi: [10.1093/mnras/staa1892](https://doi.org/10.1093/mnras/staa1892)
- Uthas, H., Knigge, C., Long, K. S., Patterson, J., & Thorstensen, J. 2011, MNRAS, 414, L85, doi: [10.1111/j.1745-3933.2011.01061.x](https://doi.org/10.1111/j.1745-3933.2011.01061.x)
- VanderPlas, J. T. 2018, ApJS, 236, 16, doi: [10.3847/1538-4365/aab766](https://doi.org/10.3847/1538-4365/aab766)
- Walters, N., Farihi, J., Marsh, T. R., et al. 2021, MNRAS, 503, 3743, doi: [10.1093/mnras/stab617](https://doi.org/10.1093/mnras/stab617)
- Warner, B. 1980, MNRAS, 191, 43P, doi: [10.1093/mnras/191.1.43P](https://doi.org/10.1093/mnras/191.1.43P)
- . 1995, Cataclysmic variable stars, Vol. 28
- Wenger, M., Ochsenbein, F., Egret, D., et al. 2000, A&AS, 143, 9, doi: [10.1051/aas:2000332](https://doi.org/10.1051/aas:2000332)
- Werner, K., Rauch, T., & Reindl, N. 2019, MNRAS, 483, 5291, doi: [10.1093/mnras/sty3408](https://doi.org/10.1093/mnras/sty3408)
- Winget, D. E., & Kepler, S. O. 2008a, ARA&A, 46, 157, doi: [10.1146/annurev.astro.46.060407.145250](https://doi.org/10.1146/annurev.astro.46.060407.145250)
- . 2008b, ARA&A, 46, 157, doi: [10.1146/annurev.astro.46.060407.145250](https://doi.org/10.1146/annurev.astro.46.060407.145250)